

VICTORIA UNIVERSITY OF WELLINGTON  
*Te Whare Wānanga o te Ūpoko o te Ika a Māui*



School of Engineering and Computer Science  
*Te Kura Mātai Pūkaha, Pūrorohiko*

PO Box 600  
Wellington  
New Zealand

Tel: +64 4 463 5341  
Fax: +64 4 463 5045  
Internet: [office@ecs.vuw.ac.nz](mailto:office@ecs.vuw.ac.nz)

**Richer Restricted Boltzmann  
Machines**

Max Godfrey

Supervisors: Marcus Fread

Submitted in partial fulfilment of the requirements for  
Bachelor of Engineering with Honours.

**Abstract**

Abstract. The abstract is your four sentence summary of the conclusions of your paper. Its primary purpose is to get your paper into the A pile. Most PC members sort their papers in an A pile and a B pile by reading the abstracts. The A pile papers get smiling interest, the B pile papers are a chore to be slogged through. By keeping your abstract short and clear, you greatly enhance your chances of being in the A pile. I try to have four sentences in my abstract. The first states the problem. The second states why the problem is a problem. The third is my startling sentence. The fourth states the implication of my startling sentence. An abstract for this paper done in this style would be: [TODO WORD-ING I or We????](#)



# Acknowledgments

Any acknowledgments should go in here, between the title page and the table of contents. The acknowledgments do not form a proper chapter, and so don't get a number or appear in the table of contents.



# Contents

<b>1</b>	<b>Introduction</b>	<b>1</b>
1.1	A Problem . . . . .	1
1.2	Deep Belief Networks can achieve state of the art performance . . . . .	1
1.3	A Proposed Solution and Contributions . . . . .	2
<b>2</b>	<b>Backgroud</b>	<b>3</b>
2.1	Generative Models . . . . .	3
2.2	Directed PGMs . . . . .	3
2.2.1	Explaining Away in DPGMs . . . . .	4
2.2.2	Directed PGMs in Neural Networks: The Sigmoid Belief Network . . . . .	5
2.3	Undirected PGMs: . . . . .	5
2.3.1	Undirected PGMs in Neural Networks: The Boltzmann Machine . . . . .	5
2.3.2	Restricted Boltzmann Machines . . . . .	6
2.4	Sampling in Generative Models . . . . .	7
2.4.1	Why sampling is important . . . . .	7
2.4.2	The sampling technique: Gibbs Sampling . . . . .	7
2.4.3	Sampling in a Sigmoid Belief Network . . . . .	8
2.4.4	Gibbs Sampling in a Boltzmann Machine . . . . .	9
2.4.5	Gibbs Sampling in RBMs . . . . .	9
<b>3</b>	<b>The ORBM: A model of independent complex causes</b>	<b>13</b>
3.1	A network equivalent to an RBM . . . . .	13
3.1.1	Unrolling a Gibbs Chain, a different perspective on RBM inference . . . . .	13
3.2	A New Approach, The ORBM . . . . .	15
3.2.1	Architecture . . . . .	15
3.2.2	Gibbs Sampling in the ORBM . . . . .	16
<b>4</b>	<b>Design and Implementation</b>	<b>19</b>
4.1	Implementation Design . . . . .	19
4.1.1	Language Choice . . . . .	19
4.1.2	Program Architecture . . . . .	20
4.1.3	Testing Approach . . . . .	20
4.2	Evaluation Design: Evaluating RBMs and ORBMs . . . . .	21
4.2.1	Hinton diagrams . . . . .	21
4.2.2	Reconstructions As a measure of Performance . . . . .	22
4.2.3	Evaluating RBMs: Problem dependent . . . . .	22
4.2.4	Evaluation Methods . . . . .	23
4.2.5	Choice of Evaluation Datasets . . . . .	24
4.2.6	Mixing Time Evaluation . . . . .	24

<b>5</b>	<b>Evaluation</b>	<b>25</b>
5.1	Two bit XOR: The minimal case . . . . .	25
5.2	Y bit pattern, X neighbouring bits on . . . . .	30
5.3	2D Patterns in a small dimensional space . . . . .	33
5.4	2D Pattern, Different Rectangle Separation . . . . .	34
5.5	MNIST Digits Mixing Time and Reconstructions . . . . .	34
5.5.1	MNIST Analysis . . . . .	36
<b>6</b>	<b>Conclusions and Future Work</b>	<b>41</b>

# Figures

1.1	An example composition of a handwritten four and three, illustrating a non-trivial task where the ground truth is known. . . . .	2
2.1	Minimal Directed PGM, showing an observed variable 'A' and it's hidden cause 'B'. . . . .	4
2.2	The famous Burglar, Earthquake, Alarm network showing a minimal case of explaining away. . . . .	4
2.3	A Boltzmann Machine, the blue shaded nodes representing the observed variables, and the non-shaded nodes the latent variables. . . . .	6
2.4	An example Restricted Boltzmann Machine with four hidden units, and five visible units. Note that the edges between units are not directed - representing a dependency not a cause. . . . .	6
2.5	A figure illustrating a Gibbs chain where left to right indicates a Gibbs iteration. Note this is <i>not</i> a PGM. . . . .	10
2.6	A diagram showing $\psi_j$ , the weighted sum into the $j$ th hidden unit. Note that $W_{0j}$ is the hidden bias, represented as a unit that is always on with a weight into each hidden unit. . . . .	11
3.1	A diagram illustrating 'unrolling' an RBM by one Gibbs iteration. Note the connections between $H$ and $V$ layers are now directed. . . . .	13
3.2	A diagram showing Ancestral sampling in the equivalent network, where normal sampling in the top 2 layers is performed until Gibbs iteration $t$ the hidden state is pushed through the bottom layers Sigmoid Network. . . . .	14
3.3	The full ORBM architecture, where $A$ and $B$ are the two causes that combine to form the data. . . . .	16
3.4	A diagram that shows the structure of the correction over the weighted sums into the hiddens of one of the RBMS versus both. Note the platuaes that are $+ - weight$ in maganitude . . . . .	18
4.1	A figure showing the architecture for the implemented test suite in UML notation. . . . .	21
4.2	Hinton Diagrams illustrating a trained hidden unit, versus that of an untrained/unutilised hidden unit. This is with no measures to enforce sparsity. . . . .	22
4.3	Bar graphs exmplifying the use of reconstructions and dreams for small numbers of RBMs. . . . .	23
4.4	A figure illustrating two five by five pixel images combining to form a composite/multicause input. The images are binary. . . . .	24
5.2	Example reconstructions for the Handcrafted RBM, For 10000 independant reconstructions given the input $[1, 0]$ . . . . .	25

5.1	The two bit RBM for modelling a single bit on at a time in a two bit pattern. The diagonal weights are negative and the non-diagonal weights are positive.	26
5.4	Dreams in the XOR RBM, note how only the training data is present. . . . .	26
5.3	The process used to create the ORBM for evalating composite XOR inputs. . .	27
5.5	The process of generating reconstruction is shown in this diagram. . . . .	28
5.6	A figure showing the result of generating 1000 reconstructions with an RBM. It is clear the RBM has no mechanism to separate the sources. Hence showing it [1,1] when it has only been trained on XOR results in no separation, i.e. reconstructions including [1,1]. . . . .	29
5.7	A figure showing interesting cases of ORBM reconstructions in $Y$ bit pattern, $X$ neighbouring bits on. . . . .	32
5.9	Figure illustrating a subset of the the results from ORBM inference on 2 By 2 square images. . . . .	33
5.10	Figure illustrating a subset of the the results from ORBM inference on 2 by 2 squares combined with $x$ by $y$ pixel rectangles. . . . .	34
5.8	A figure illustrating the dataset used for this task. 2 by 2 pixel squares in a 5 by 5 pixel image. . . . .	34
5.11	Mixing Time . . . . .	37
5.12	Dataset-wide MNIST Score Results . . . . .	38
5.13	Cosine Score breakdown for the highest and lowest performing datasets, 0 and 9. . . . .	38
5.14	Best Scores . . . . .	39
5.15	Worst Scores . . . . .	39



# Chapter 1

## Introduction

### 1.1 A Problem

Consider an image of a face. At least two *systems* are at play in the image of a face, the face itself and the illumination. Both face and illumination are complex and can vary greatly, but they are fundamentally acting independently of each other up until they compose to form the image.

A form of Deep Neural Networks, Deep Belief Networks, have achieved state of the art performance in facial recognition, but this is only possible with a large amount of training data. This suggests that there is a disparity between the task and these networks, as the networks do not explicitly attempt to represent these *systems* independently. This project takes steps toward representing complex causes separately with the primary task of decomposing joint images (more generally, vector based data).

Separating faces and illumination is too challenging for this project, there is no way to verify/evaluate that the new approach is working as the concept of a face without illumination cannot be visualised. Instead I will start with the modest task of working with images where the source images being combined are known.

### 1.2 Deep Belief Networks can achieve state of the art performance

Deep Belief networks (DBNs) are powerful models that have proven to achieve state of the art performance in tasks such as image classification, dimensionality reduction, natural language recognition, Document classification, Semantic Analysis. **TODO CITE:** Despite a DBN's expressiveness, there is no way to extract independent sources, the model instead learns how to represent the complex combination. The complex combination of sources is inherently richer than the individual sources acting alone. The DBN may learn features that correspond to each source during its training process, however the architecture or training algorithm make no attempt to enforce this. Consider face and illumination example, with 1000 possible faces and 1000 possible illuminations. If we only observe a combination of faces and illuminations there is 1000000 possible combinations we need to represent. It is more succinct to treat faces and illumination as independent *system*, resulting in 2000 combinations.

DBNs are built of shallow networks called Restricted Boltzmann Machines (RBMs). Despite being building blocks for the DBN RBMs can be used as models for practical tasks for instance representing handwritten digits [2].

### 1.3 A Proposed Solution and Contributions

Frean and Marsland propose an alternative architecture to that of an RBM, that aims to encode two complex sources independantly. Frean and Marsland also propose an algorithm to put this alternative architecture to use.

This project contributes:

- C1. The first articulation of the proposed architecture, including the context needed to understand it.
- C2. A Python implementation of the new architecture.
- C3. A suite of graded evaluations/tests that explore how the architecture and source separation algorithm work in practice.

The evaluations will not address separating faces and illumination, instead the more general case of two images overlaying to form the data. The implications of this are compelling as applications could include removing noise from images or extracting images that are composed of many subjects. These are aspirational goals and this project will only performing tasks such as separating two handwritten digits composed on each other (see figure 1.1).



Figure 1.1: An example composition of a handwritten four and three, illustrating a non-trivial task where the ground truth is known.

# Chapter 2

## Backgroud

As the proposed architecture and algorithm extend existing work on Probablistic Graphical Models, a substantial amount of background is required culminating with the new approach being derived. An robust understanding of these concepts is required for this project to implement and design appropriate evaluations for the proposed architecture new approach.

### 2.1 Generative Models

This project works with nueral network based generative models. Generative models are a powerful way to model data. The rational behind them being that we aim to learn a model that can both create the training data represent it, and reconstruct it using it's learned representation. Generative models can map input data from raw values to higher level features. Hinton [4] gave a compelling argument for higher level features in the context of generative models.

Consider, for example, a set of images of a dog. Latent variables such as the position, size, shape and color of the dog are a good way of explaining the complicated, higher-order correlations between the individual pixel intensities, and some of these latent variables are very good predictors of the class label.

Generative models model a distribution over a collection binary variables  $X$ , where  $X$  is comprised of variables which can be observed or unobserved. The observed variables are referred to as `visible` variables or units ( $v$ ). Conversely, unobserved variables correspond to the hidden units of the neural network ( $h$ ). With these terms defined the joint distribution that generative models model can be expressed as  $P(X)$  where  $X$  is comprised of  $h, v$ . Collections of these units, are often referred to as 'patterns' or 'vectors' in that they are represented by a vector or pattern of bits. For instance in the context of an image, a visible pattern is the pixels of the image flattened into a one dimensional vector.

### 2.2 Directed PGMs

The new approach proposed in this project uses both the two classes of Probablisitic Graphical Models, Directed and Undirected. A Directed PGM, is a notation for factorising over a collection of stochastic variables. Given  $X$ , the variables in the generative model, and  $parent_i$  the parent unit of  $x_i$ , the distribution over  $X$  in a directed PGM is defined by the following factorisation:

$$P(X) = \prod_i P(x_i | parent_i) \quad (2.1)$$

Connections between units in the Directed PGM express causation [13]. They provide an expressive way to represent a collection of related, stochastic variables. See figure 2.1 for the minimal example, where variable  $A$  is dependent on  $B$ . As a result this network is often referred to as a Belief Network or Bayesian Network where its causal dependencies are expressed as a conditional probability table or ‘factor’. For example in figure 2.1 the probabilities of  $A$  being in a given state are dependent on  $B$ . The joint distribution over  $A$  and  $B$ , as in equation 2.1, can be expressed as:

$$P(A, B) = P(A|B)P(B)$$

TODO WORDING consider removing — Note that a normalisation is not needed in DPGMs as the conditional probabilities enforce that the factors sum to 1.

### 2.2.1 Explaining Away in DPGMs

TODO WORDING A common task in generative models is given a known parent unit (a cause), is inferring the probability of children variable dependent on that parent being in a given state. In directed PGMs this proves trivial to calculate. The opposite task of inferring the state of causes, given the effect of that cause is also a desirable task. It becomes problematic in DPGMs as these causal relationships give rise to the effect of ‘Explaining Away’. The canonical example Burglar, Earthquake, Alarm Problem is a exemplifies this effect effect[1] and is illustrated in figure 2.2. Knowledge of the state of the alarm makes

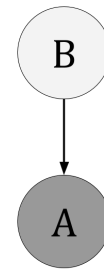


Figure 2.1: Minimal Directed PGM, showing an observed variable ‘A’ and its hidden cause ‘B’.

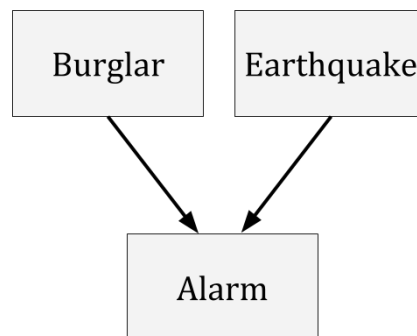


Figure 2.2: The famous Burglar, Earthquake, Alarm network showing a minimal case of explaining away.

burglar and earthquake dependent. The alarm is the observable variable here ( $v$ ) and the burglar and earthquake are the hidden ‘causes’ ( $h$ ). For example if the alarm is true, and we see news of earthquake in the area, our belief that we have been burgled decreases. Expressed (again exemplify equation 2.1) in probabilities where  $A$ ,  $B$  and  $E$  are the states of alarm, burglar and earthquake respectively:

$$P(A, B, E) = P(A|B, E)P(B)P(E)$$

### 2.2.2 Directed PGMs in Neural Networks: The Sigmoid Belief Network

A Belief network can be expressed as a neural network, where conditional probabilities are parameterised as weights. **TODO WORDING Simplify** — This network is called a Sigmoid Belief Network (SBN) as the probability of a variable  $x_i$  being 1 that is dependent on an ancestor variable  $parent_i$  the weighted sum into  $x_i$ ,  $\phi_i$  passed through the sigmoid function ( $\sigma(x) = 1/(1 + e^{-x})$ ). This is equivalent to a perceptron using a sigmoid activation function and ensures that the output is a valid probability (between 0 and 1). SBNs take a naive approach to causes, where each hidden unit represent a single, simple cause. Formally,  $\phi_i$  is a weighted sum of the activations of parent nodes:

$$\phi_i = \sum_{j \in parent_i} W_{ij} x_j$$

and

$$P(x_i = 1 | parent_i) = \sigma(\phi_i)$$

### 2.3 Undirected PGMs:

Undirected PGMs do not represent causation, instead merely capturing a dependency between two units. These pairwise dependencies change the structure of the factorisation a factor  $\Phi$  between each pair of variables  $x_i, x_j$  resulting in the factorisation:

$$P(X) = \frac{1}{Z} \prod_i \Phi(x_i, x_j)$$

The introduction of the normalisation  $Z$  (often referred to as the partition function) adds nontrivial complexity to performing inference in Undirected PGMs **TODO CITE** , a sum over all  $2^N$  configurations of  $x$  is required.

On the other hand, Undirected PGMs do not capture causal relationships. Calculating the state of a variable given another is no longer hampered by the effect of explaining away, however their recurrent structure, while expressive introduces an intractability in practice.

#### 2.3.1 Undirected PGMs in Neural Networks: The Boltzmann Machine

A UPGM expressed as a neural network is referred as Boltzmann Machine or Markov Field, where connections encode dependencies with an associated weight. We see this where  $W_{ij}$  is the weight between variables  $x_i$  and  $x_j$  the factor  $\Phi$  is expressed as:

$$\Phi(x_i, x_j) = e^{x_i x_j W_{ij}}$$

The Boltzmann machine has proposed in various forms, from different domains throughout the years, for instance it was presented in a non-stochastic context of the Hopfield network in [8]. Hinton and Sejnowski also proposed the Boltzmann machine in [6]. An example Boltzmann Machine is shown in figure 2.3. As shown in this figure 2.3, the Boltzmann Machine can be recurrent, expressing complex dependencies between variables. This recurrence makes inferring the state of a subset variables based on knowledge of another subset non-trivial as the size of the network grows **TODO CITE** .

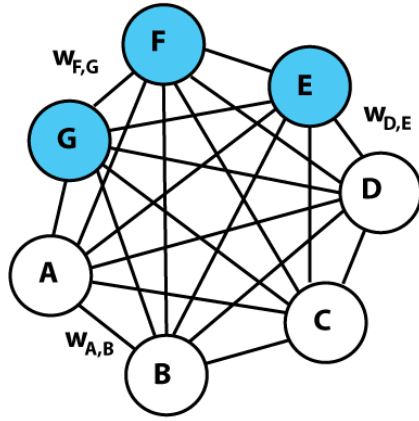


Figure 2.3: A Boltzmann Machine, the blue shaded nodes representing the observed variables, and the non-shaded nodes the latent variables.

### 2.3.2 Restricted Boltzmann Machines

TODO WORDING A Boltzmann Machine's architecture can be altered to alleviate inference shortcoming. The restriction, originally proposed by [14], and then later revitalised with a training algorithm that operates on the deeper architecture of the DBN [6]. The restriction requires the network to be a two layer bipartite network, each layer corresponding to the observed (visible) and latent (hidden) units. Connections are forbidden between the layer of hidden units and the layer of visible units respectively. An example Restricted Boltzmann Machine architecture is shown in figure 2.4. The collection of hidden units, forming a layer are referred to as the hidden layer. The collection of visible units are referred to as the visible layer.

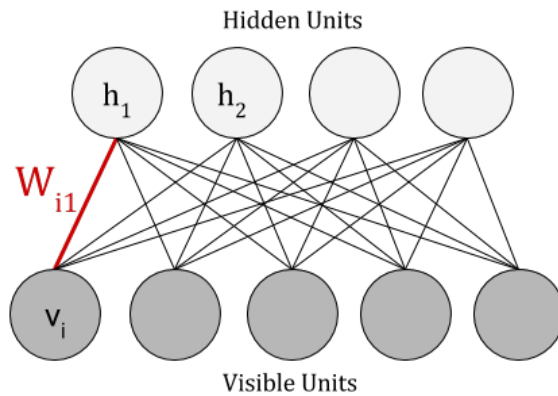


Figure 2.4: An example Restricted Boltzmann Machine with four hidden units, and five visible units. Note that the edges between units are not directed - representing a dependency not a cause.

The probability of the RBM being in a given configuration is the joint probability of  $h$  and  $v$ :

$$P(h, v) = \frac{1}{Z} \prod_{j,i} e^{h_j v_i W_{ji}}$$

Taking logs this becomes:

$$\log P(h, v) = \log \sum_{j,i} h_j v_i W_{ji} - \log Z$$

$Z$  is the partition function, which normalises the probability of the joint. Calculating this would require summing over all  $2^N$  configurations of  $h$  and  $v$ , which is intractable for practical numbers of units. For instance a 28 by 28 image corresponds to 784 visible units, and for, say 10 hidden units this would amount to  $2^{784} * 2^{10}$  possible configurations. We opt to work in terms of  $P^*$  which is the non-normalised probability of the joint over  $h$  and  $v$ .

$$\log P^*(h, v) = \log \sum_{i,j} h_j v_i W_{ji} \quad (2.2)$$

## 2.4 Sampling in Generative Models

### 2.4.1 Why sampling is important

Sampling is used when the distribution we want to work from is intractable to calculate analytically. As mentioned in 2.1, the power of generative models is their ability to represent, reconstruct and be trained on data. These tasks all require sampling from configurations of the hidden and visible units, often conditioned one or the other. There are two cases:

- Sampling from  $P(v|h)$ , which is known as running the generative model, where the model *generates* data based on a hidden representation.
- Sampling from  $P(h|v)$ , which is known as *inverting* a generative model (This is also referred to as *inference*). The process is called ‘Inverting’ because instead of the model generating the data (sampling from  $P(v|h)$ ) we instead try to infer a representation given data  $P(h|v)$ . It is the process of reasoning about what we do not know, given that of which we do.

Sampling from  $P(v|h)$  and  $P(h|v)$  is required to train generative models, as often the gradient to be climbed/descended involves calculating a probability over all the units in the generative model. Training a network based generative model involves calculating a weight update, which in turn requires inferring a hidden representation given a training item. The converse, sampling from a  $P(v|h)$  is also required. **TODO CITE: EM**

**TODO WORDING** inference for our purpose is used for (something about not training)

### 2.4.2 The sampling technique: Gibbs Sampling

Gibbs sampling is a special case of Markov Chain Monte Carlo [3], a technique for drawing sampling from a complex distribution. Sampling from the probability mass (or ‘joint distribution’) of a generative model is a common use case for Gibbs sampling [12].

Gibbs sampling explores the desired probability distribution, taking samples of that distribution’s state, allowing iterations of exploration between drawing of a sample to ensure that the samples are independent**TODO CITE: .** The process of taking a step between states is referred to as a Gibbs iteration or a Gibbs Step. Formally the algorithm is described in algorithm 1.

**Data:** A vector  $x$  indexed by  $j$ .  
**Result:** Gibbs sampling algorithm  
Let  $x_{\setminus j}$  be all components that make up  $x$  vector except  $x_j$ ;  
initialization, begin with  $x$ , we are going to get a sample  $x'$ ;  
**for**  $k$  many iterations **do**  
    **for** each component in  $x$ ,  $x_j$  **do**  
        Draw a sample,  $x'_j$  from  $P(x_j|x_{\setminus j})$ ;  
        Update the current value of  $x_j$  in  $x$  with  $x'_j$ ;  
    **end**  
**end**

**Algorithm 1:** The Gibbs Sampling Algorithm

### Mixing Time of the Gibbs Sampler

MCMC methods aim to approximate a distribution, by exploring likely states. As we often start this process from a random state, it's important that enough Gibbs steps are taken before a sample is drawn. This is because the random state may not be close any part of the true distribution we want to sample from, so by running the chain for many iterations we increase the likelihood of samples being from the desired distribution.

This process of waiting for enough steps to before drawing samples is referred to as the Mixing Time. When Hinton when proposed a fast training for algorithm for RBMs and DBNs [5], Gibbs sampling is used for performing inference in RBMs and as result also in the ORBM. The mixing time, that is how many Gibbs iterations are needed to reach a satisfactory sample is an important part issue in the ORBM, in that one Gibbs step was sufficient in practice for training and using an RBM. The new generative model is not so fortunate.

### 2.4.3 Sampling in a Sigmoid Belief Network

Sampling from  $P(v|h)$  (known as Ancestral Sampling) is extremely efficient in a SBN, it does not need Gibbs sampling. It can be expressed as

$$P(v|h) = \sum_i v_i \log \sigma_i(h) + (1 - v_i) \log(1 - \sigma_i(h)) \quad (2.3)$$

As this process is calculated by propagating probabilities from the root hidden causes, it is known in a SBN as Ancestral Sampling.

Conversly, sampling from  $P(h|v)$  in an SBN is intractable. Performing inference in a Sigmoid Belief network would allow source separation, as each hidden unit could represent a simple cause. The SBN would be shown an input, and could extract representations of the seperate causes that likely gave rise to the input. There exist algorithms for performing inference in Sigmoid Belief Networks. For instance, the Belief Propagation algorithm proposed by Judea Pearl [11] operates on this encoding, calculating the probabilities of a given network state (i.e. the state of all the variables). As well as constraining the architecture to be Directed Acyclic Graph, Belief Propagation is intractable to use as the number of variables grow **TODO CITE**. As we want to work with cases with upwards of 100 visible and hidden nodes, these algorithms break down.

Despite the Sigmoid Belief Network being expressive and providing a succinct encoding of conditional probabilities, Gibbs sampling is intractable for SBNs of practical size [9]. The issue being that the Gibbs chain takes too long to mix [10], which arises from the the 'explaining away effect' [5]. Calling back to the example in section ??, instead of a single



burglar or earthquake becoming dependant given the alarm, there is more in the realm of hundreds of burglars and earthquakes all suddenly dependant.

Being able to efficiently sample from  $P(h|v)$  is also required for training generative models [TODO CITE: em](#) making Sigmoid Belief Networks impractical for not only inference, but also training.

#### 2.4.4 Gibbs Sampling in a Boltzmann Machine

Performing Gibbs sampling appears trivial in a Boltzmann Machine, in that to find the probability of a given unit being active a weighted input to that node is passed through a sigmoid function. However, in practice the recurrent nature of Boltzmann Machines makes sampling intractable as updating a node will change the probabilities of those connected. However, it was shown that given unlimited training time Boltzmann Machines could be trained, outperforming the state of the art models of the time [TODO CITE: This](#).

Recall that  $x_{\setminus j}$  be all components that make up  $x$  vector except  $x_j$  and that a Boltzmann Machine has symmetric weights ( $W_{ji} = W_{ij}$ ),

$$P(x_j = 1, x_{\setminus j}) = \frac{1}{1 + e^{-\sum_i w_{ji} x_i}}$$

That is, Gibbs sampling in a Boltzmann Machine amounts to use the Sigmoid function of the weighted inputs. [TODO CITE: neal1992:connectionist](#)

#### 2.4.5 Gibbs Sampling in RBMs

A big payoff for the restriction in an RBM is inverting the model becomes tractable, as the latent variables no longer become dependant given the observed variables. This is illustrated in figure 2.4 the hidden unit  $h_1$  is not dependent on  $h_2$  whether or not we know anything about the visible units. Firstly, this is the opposite of a SBN, where knowledge of the visible units makes the hidden units dependant. Secondly, by removing the recurrence present in Boltzmann Machines, it reduces the expressiveness of the RBM network while making the RBM useable in practice as the Gibbs sampling process can stop after one Gibbs step [TODO CITE: .](#)

In order to describe Gibbs sampling in the new architecture proposed, it must first be explained for a standard RBM — The process of Gibbs sampling is as follows:

- One must sample from  $P(h|v)$  giving a hidden state  $\tilde{h}'$
- Using this hidden state, a visible state is then generated,  $\tilde{v}'$ , by sampling from  $P(\tilde{v}'|\tilde{h}')$ . This process of generating a hidden pattern, and subsequent visible pattern is referred to as a Gibbs step.
- This chain of Gibbs steps between sampling from  $P(h|v)$  and  $P(v|h)$  can then be repeated as desired, the longer the chain the closer the samples will be to the true joint distribution that the model has learnt. For training an RBM Hinton [TODO CITE: CD-1Paper](#) showed that 1 step is often enough in practice, as one step is enough to infer a direction to adjust the weights in.

The process of updating the hidden, then visible layers forms what is referred to as the Gibbs Chain and is visualised at layer level in figure 2.5.

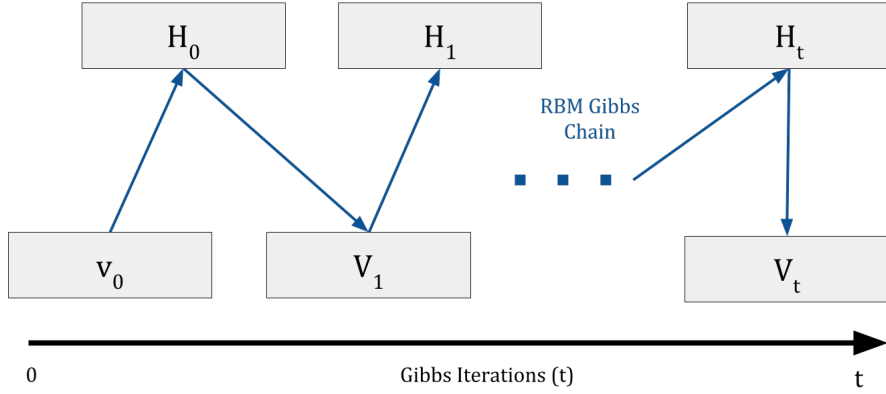


Figure 2.5: A figure illustrating a Gibbs chain where left to right indicates a Gibbs iteration. Note this is *not* a PGM.

### The Gibbs update

Denote the Gibbs sampler's probability of setting a variable,  $x_j$  to 1 as:

$$P_{Gibbs}(h_j = 1|v, h_{k \neq j}) \quad (2.4)$$

We can refer to the probability in equation 2.4 as  $p_1$  and the converse  $P_{Gibbs}(h_j = 0|v, h_{k \neq j})$  can be referred to as  $p_0$ . Then, by the product rule of probabilities:

$$\begin{aligned} \frac{p_1}{p_0} &= \frac{P^*(h, v \text{ where } h_j = 1)}{P^*(h, v \text{ where } h_j = 0)} \\ &= \frac{p_1}{1 - p_1} \\ p_1 &= \frac{1}{1 + \frac{P^*(h, v \text{ where } h_j = 0)}{P^*(h, v \text{ where } h_j = 1)}} = \frac{1}{1 + e^{-\psi_j}} \end{aligned}$$

To update a hidden unit  $h_j$  we find  $P(h_j = 1|v)$  where  $v$  is an input pattern. In the context of an image,  $v$  would be the pixel values where each pixel corresponds to a visible unit,  $v_i$ . The probability of a given hidden unit activating is: **TODO CITE: Gibbs sampling would be good here.**

$$P(h_j = 1|v) = \sigma(\psi_j) \quad (2.5)$$

Where  $\psi_j$  is the weighted sum into the  $j$ th hidden unit and  $\sigma()$  is the Sigmoid function, or it also known as the Logistic function  $\sigma(x) = 1/(1 + e^{-x})$ . Figure 2.6 illustrates  $\psi_j$  for an example RBM. As the weights are symmetric, sampling from the visible layer, given a hidden state is similar. That is  $P(v_i = 1|h)$ , where  $h$  is the entire hidden vector is given by:

$$P(v_i = 1|h) = \sigma(\phi_i) \quad (2.6)$$

Where  $\phi_i$  is the weighted sum into the  $i$ th visible unit, which is:  $\phi_i = \sum(W_{ji}h_j) + W_{0i}$ . Both  $\phi_j$  and  $\psi_i$  can be expressed in alternative, but useful way:

$$\phi_j = \log P^*(v, h|v_i = 1) - \log P^*(v, h|v_i = 0) \quad (2.7)$$

$$\psi_i = \log P^*(h, v|h_j = 1) - \log P^*(h, v|h_j = 0) \quad (2.8)$$

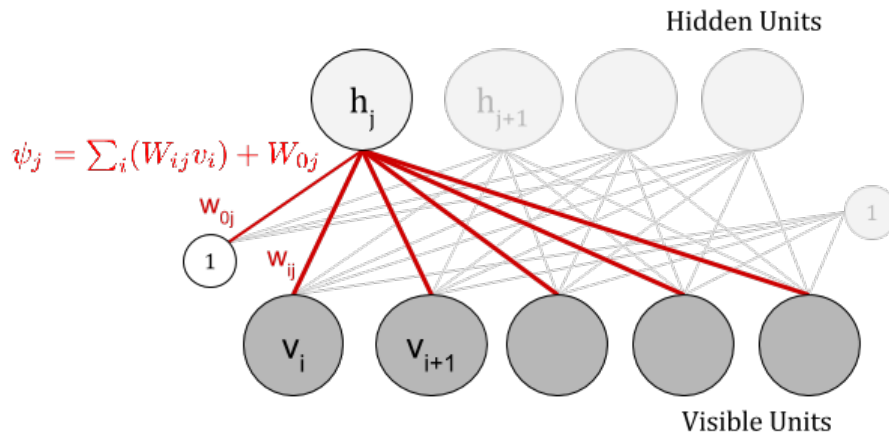


Figure 2.6: A diagram showing  $\psi_j$ , the weighted sum into the  $j$ th hidden unit. Note that  $W_{0j}$  is the hidden bias, represented as a unit that is always on with a weight into each hidden unit.

### Reconstructions: visualising what the RBM has learnt

RBM's create an internal representation given an input by sampling from  $P(h|v)$ . They can also generate a faux input given an internal representation. Performing one Gibbs iteration, that is, sampling from the hidden units given a 'clamped' input  $P(h|v)$  and then taking the generated hidden state and generating a faux input (sampling from  $P(v|h_{\text{sampled}})$ ) results in a reconstruction. Clamped input is where the visible units are set to be an input pattern. The model tries to reconstruct the input based on the internal representation it has learnt to model. This has applications in increasing the size of a dataset by introducing variation by generating these faux inputs **TODO CITE: .**

### RBM Fantasies: The Free-Phase of a Generative model

In the same way that a Generative model uses reconstructions to try and recreate the supplied input vector, performing many, many (greater than 100) Gibbs iterations with no input pattern clamped allows the reconstructions to explore the probability mass that has been built by the model during training. Sampling from these wanderings creates what are referred to as 'fantasies' or 'dreams'. These give a sense of what the model has learnt, and can act as a smoke test for if the model has actually captured anything. **TODO CITE: (TODO-CITE-PAPER-WITH-MNIST-DREAM-EVALUATION, they were crappy).**



## Chapter 3

# The ORBM: A model of independent complex causes

### 3.1 A network equivalent to an RBM

#### 3.1.1 Unrolling a Gibbs Chain, a different perspective on RBM inference

Before the ORBMs architecture and inference algorithm can be introduced, Gibbs sampling in an RBM must be presented in a different, yet equivalent way. Hinton, when introducing the idea of training a Deep Belief Network showed that a Gibbs chain in an RBM is equivalent to a infinitely deep belief network, with an RBM on the top with tied weights. **TODO CITE: Hinton's paper on unrolling the Gibbs chain.** An unrolling of a single Gibbs iteration is illustrated in figure 3.1, the  $U$  layer corresponding to the  $V$  layer after one Gibbs iteration.

The top two layers ( $U$  and  $H$ ) form a standard RBM, but the bottom connections ( $V$  and  $H$ ) form a Sigmoid Belief Network. To further clarify, the  $U$  layer corresponds to  $V_1$  in figure 2.5. Note in figure 3.1 the weights between the  $H$  and  $U$  layer are shared between the  $V$  and  $H$  layers.

We can now show that Gibbs sampling in this RBM unrolled with a Sigmoid belief network is equivalent to Gibbs Sampling in a standard RBM.

#### Sampling in this equivalent network

sampling in the ORBM **TODO CITE: as described in the section where I talk about dreams...** network behaves a similar way to RBM sampling, where a Gibbs chain is run between the top two layers,  $U$  and  $H$ , until the last iteration. At the last iteration a hidden pattern is

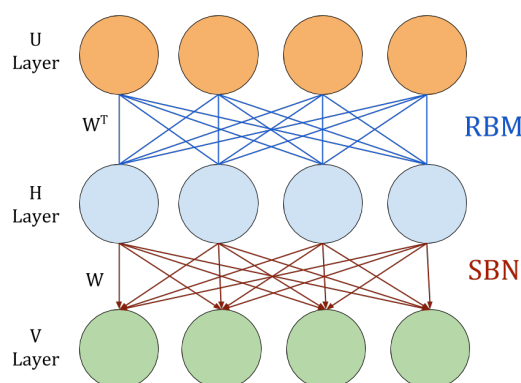


Figure 3.1: A diagram illustrating 'unrolling' an RBM by one Gibbs iteration. Note the connections between  $H$  and  $V$  layers are now directed.

sampled and then is pushed through the Sigmoid belief network between  $H$  and  $V$ . This is illustrated in figure 3.2.

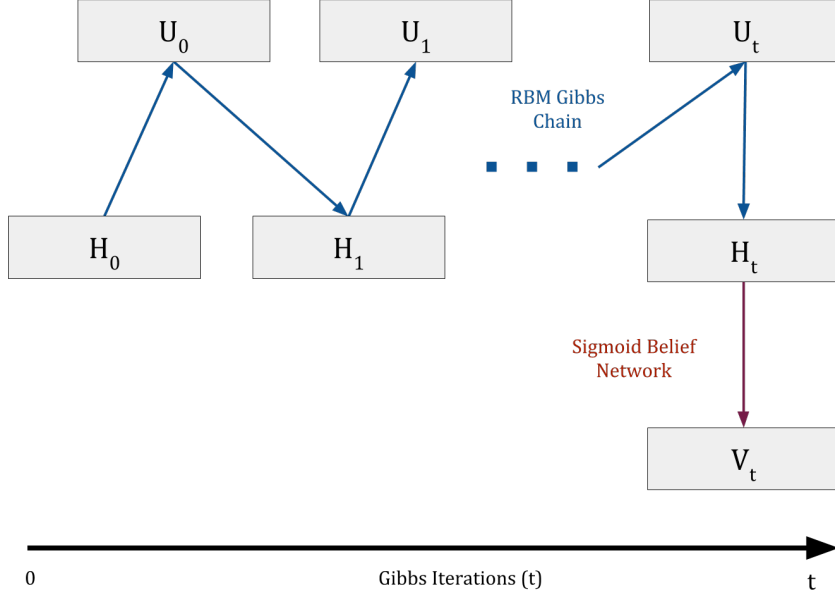


Figure 3.2: A diagram showing Ancestral sampling in the equivalent network, where normal sampling in the top 2 layers is performed until Gibbs iteration  $t$  the hidden state is pushed through the bottom layers Sigmoid Network.

To generate a sample from  $h$  is equivalent we can use equation 2.5, by running the Gibbs chain between  $h$  and  $U$ . To sample from  $v$  in the SBN is by definition:

$$P(v_i = 1|h) = \sigma_i(h)$$

Thus Gibbs sampling from a simple RBM ending in a sample for  $v$  is the same as sampling  $h$  from the same RBM and using a SBN for the last step.

There is however another useful way to draw samples in such a network that we will leverage in the ORBM. The log likelihood of the joint can be written as:

$$\log P^*(h, v) = \log P^*(h) + \log P(v|h) \quad (3.1)$$

The second term is defined in equation 2.3. To find the first term,  $P^*(h)$ , we need to marginalise the joint (eq 3.1) over all  $U$  layer configurations:

$$\begin{aligned}
P^*(h) &= \sum_{v_1=0}^1 \cdots \sum_{v_n=0}^1 \exp \left[ \log P^*(h, v) \right] \\
&= \sum_{v_1=0}^1 \cdots \sum_{v_n=0}^1 \exp \left[ \sum_i \sum_j h_j W_{ji} v_i + \sum_i W_{0i} v_i + \sum_j W_{j0} h_j \right] \\
&= \sum_{v_1=0}^1 \cdots \sum_{v_n=0}^1 \exp \left[ \sum_i v_i \phi_i(h) + \sum_j W_{j0} h_j \right] \\
&= \exp \left[ \sum_j h_j W_{j0} \right] \times \sum_{v_1=0}^1 \cdots \sum_{v_n=0}^1 \prod_i \exp \left[ v_i \phi_i(h) \right] \\
&= \exp \left[ \sum_j h_j W_{j0} \right] \times \prod_i \left( 1 + e^{\phi_i(h)} \right)
\end{aligned}$$

and taking logs,  $\log P^*(h) = \sum_j h_j W_{j0} + \sum_i \log \left( 1 + e^{\phi_i(h)} \right)$

$$= \sum_j h_j W_{j0} + \sum_i \phi_i(h) - \sum_i \log \sigma_i(h)$$

So far we've figured out  $\log P^*(h)$  for the RBM that is the 'top layer'.

Therefore another way to write  $\log P^*(h, v)$  is

$$\log P^*(h, v) = \underbrace{\sum_j h_j W_{j0} + \sum_i \phi_i(h) - \sum_i \log \sigma_i(h)}_{\log P^*(h)} + \underbrace{\sum_i v_i \log \sigma_i(h) + (1 - v_i) \log(1 - \sigma_i(h))}_{\log P(v|h)} \quad (3.2)$$

By collecting terms and simplifying this matches the earlier form in equation 2.2.

## 3.2 A New Approach, The ORBM

### 3.2.1 Architecture

Frean and Marsland extend on this idea of a one Gibbs iteration unrolled RBM. They propose adding another  $U$  and  $H$  layers to represent another rich source of data, which then combines with the original  $U$  and  $H$  layer via a SBN to form  $V$ . This architecture is illustrated in figure 3.3, where A and B are used to denote the two independent causes we are modeling. To clarify the ORBMs architecture, there are two RBMs, one for each cause. These RBMs are connected to a SBN into the visible layer, the weights of which are tied to the respective RBMs. This architecture is simpler in practice as the  $U$  layers can be captured in the inference algorithm.

By building on RBMs and SBN we can leverage existing algorithms and work on RBMs and also the potential for extending this work to deeper architectures is possible. Also the architecture supports 'plug and play' with the models in that existing RBMs can be plugged into the architecture. The implications of this are exciting in that an RBM that has been trained on hand written digits could be plugged into an RBM that has been trained on a paper texture (the bumps and ridges of paper). Then using the ORBM a 'clean' representation of the text and paper could be separated out given an image of a digit on paper.

The ORBM, like the RBM is difficult to evaluate empirically, but the same techniques that can be used to evaluate RBMs can be applied to the ORBM.

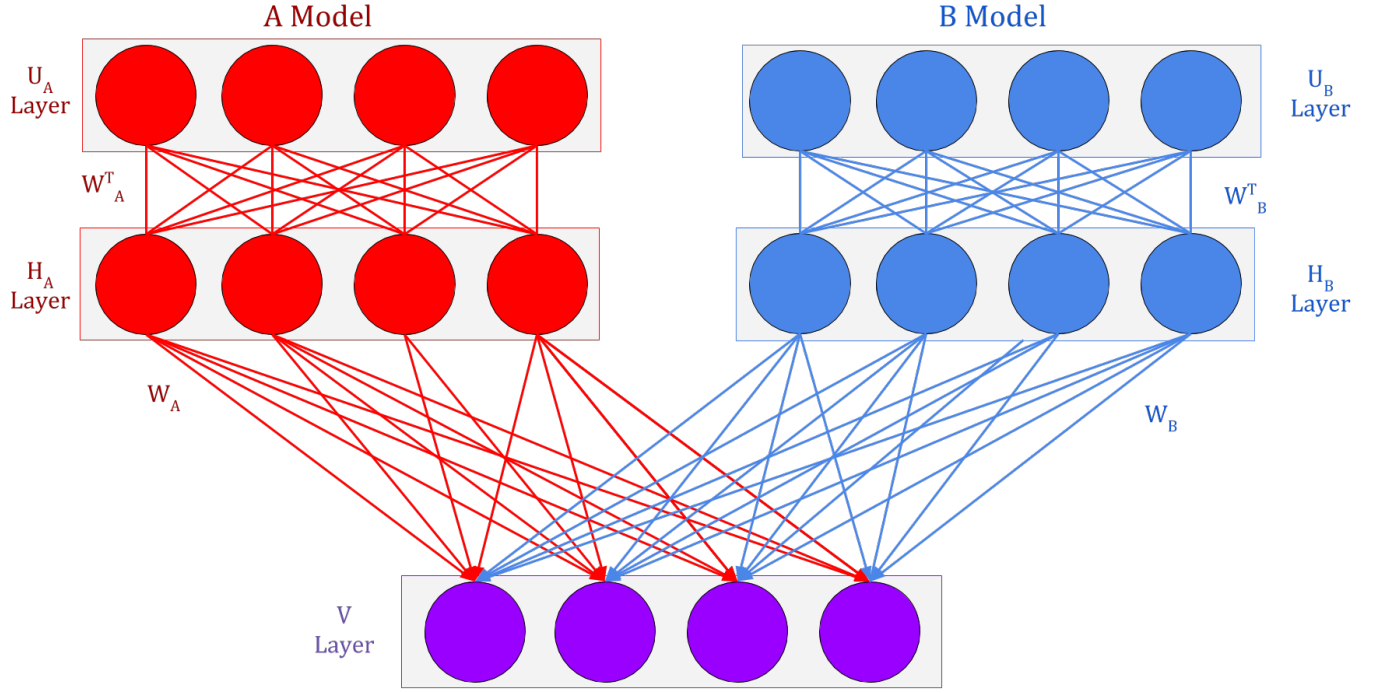


Figure 3.3: The full ORBM architecture, where  $A$  and  $B$  are the two causes that combine to form the data.

### 3.2.2 Gibbs Sampling in the ORBM

#### Ancestral Sampling in the ORBM

Ancestral sampling in an RBM involved running a Gibbs chain and then taking the last visible in that chain. To perform ancestral sampling in the ORBM we can leverage the generative power of the RBM and then combine their inputs in a simple way. We know that joint in the unrolled RBM is expressed as eq 3.1. That is, the ORBM probability of  $v$  given  $h^A$  and  $h^B$  is defined by:

$$\log P(v|h^A, h^B) = \sum_i v_i \log \sigma(\phi_i^A + \phi_i^B) + (1 - v_i) \log(1 - \sigma(\phi_i^A + \phi_i^B))$$

Where  $\phi_i^A$  and  $\phi_i^B$  are the weighted sums into the  $i$ th visible units from the models  $A$  and  $B$  respectively. In this generative model a visible unit is created by taking the weighted sum from both sources, adding their contribution and then passing through a Sigmoid function to give a probability.

#### Inference in the ORBM

In a standard RBM sampling from  $P(h_j)$  is given by  $P(h_j) = \sigma(\psi_i)$ , where  $\psi_i$  is defined in equation 2.8. In an ORBM we cannot consider the single RBM alone when trying to find  $P(h_j)$ , as the hidden layers of the two RBMs in the ORBM are dependent given a visible layer  $v$ . This amounts to explaining away as described in section ???. There is a nice feature of the ORBM in that the hidden representations ( $h^A$  and  $h^B$ ) we extract from the visible layer require no interaction with the  $U$  layers to sample from. They are only needed to generate a composite  $V$  pattern (or independent reconstructions).



We aim to use Gibbs sampling to generate  $h^A$  and  $h^B$  given a  $v$ : We need to calculate

$$\psi_j^A = \log P^*(h, v | h_j^A = 1) - \log P^*(h, v | h_j^A = 0)$$

We will use that fact that the weighted sum into a visible unit  $i$  where some hidden unit  $h_j$  is on, is equivalent to the same configuration except  $h_j$  is off plus the weight between these two units. This is by definition true, and expressed below:

$$\phi_i^A(h | h_j^A = 1) = \phi_i^A(h | h_j^A = 0) + W_{ji}^A$$

We will abbreviate  $\phi_i^A(h | h_j = 0)$  to  $\phi_i^{Aj0}$ . Given these we obtain:

$$\psi_j^A = \sum_i v_i \log \left( \frac{1 + e^{-\phi_i^{Aj0} - \phi_i^B}}{1 + e^{-\phi_i^{Aj0} - W_{ji} - \phi_i^B}} \frac{1 + e^{\phi_i^{Aj0} + W_{ji} + \phi_i^B}}{1 + e^{\phi_i^{Aj0} + \phi_i^B}} \right) + \sum_i \log \left( \frac{1 + e^{\phi_i^{Aj0} + W_{ji}}}{1 + e^{\phi_i^{Aj0}}} \frac{1 + e^{\phi_i^{Aj0} + \phi_i^B}}{1 + e^{\phi_i^{Aj0} + W_{ji} + \phi_i^B}} \right)$$

Now  $\phi = \log \frac{1+e^\phi}{1+e^{-\phi}}$  (Marcus' magic identity), which is  $= \log \frac{\sigma(\phi)}{\sigma(-\phi)}$ . So the first term simplifies to  $\sum_i v_i W_{ji}$ , which is the same as that in an RBM. The second term can also be simplified, using the identity  $\log(1 - \sigma(\phi)) = \phi - \log(1 + e^\phi)$ . This leads to the following Gibbs Sampler probability of the  $j$ -th hidden unit in network  $A$  being 1:  $p_j = \sigma(\psi_j^A)$  with

$$\psi_j^A = \underbrace{\sum_i W_{ji}^A v_i}_{\text{vanilla RBM}} + \underbrace{\sum_i C_{ji}^A}_{\text{correction}}$$

where the correction is:

$$\begin{aligned} C_{ji}^A &= \log \left[ \frac{\sigma(\phi_i^{Aj0})}{\sigma(\phi_i^{Aj0} + W_{ji}^A)} \cdot \frac{\sigma(\phi_i^{Aj0} + W_{ji}^A + \phi_i^B)}{\sigma(\phi_i^{Aj0} + \phi_i^B)} \right] \\ &= \log \sigma(\phi_i^{Aj0}) + \log \sigma(\phi_i^{Aj0} + W_{ji}^A + \phi_i^B) - \log \sigma(\phi_i^{Aj0} + W_{ji}^A) - \log \sigma(\phi_i^{Aj0} + \phi_i^B) \\ &= \log \left[ \frac{\sigma(\phi_i^A - h_j^A W_{ji}^A)}{\sigma(\phi_i^A + (1 - h_j^A) W_{ji}^A)} \right] - \log \left[ \frac{\sigma(\phi_i^{AB} - h_j^A W_{ji}^A)}{\sigma(\phi_i^{AB} + (1 - h_j^A) W_{ji}^A)} \right] \end{aligned} \quad (3.3)$$

where  $\phi_i^{AB} = \phi_i^A + \phi_i^B$ . Note that  $v$  plays no role in the correction. It is clear that adding  $\phi_i^B$  has introduced a dependency between the entirety of  $h$ . This means that a Gibbs chain will need to be run, in practice this chain proves to be short, even in the larger dimension tasks like MNIST.

### Examining and approximating the Correction

This correction (eq 3.3) is a non-trivial computation to make in that for every weight, a series of semi-large matrix operations have to be performed. As a result, Freat and Marsland propose an approximation for this correction.

It is useful to see the correction contours on axes  $\phi_i^A$  versus  $\phi_i^{AB}$ , for a positive weight  $W_{ji}^A$ . There are two plots for the two cases  $h_j^A = 0$  and  $h_j^A = 1$  These are plotted in figure 3.4. This function has defined 'plateaus' where the height of these plateaus is  $\pm$  the weight respectively. The correction essentially adjusts the weight between  $v_i$  and  $h_j$  allowing it to be turned off, turned on, intensified, deintensified, or have no effect. This is similar to adjusting the visible activation based on what the two RBMs are doing and hence Freat and Marsland propose the following approximation:

$$C_{ji}^A = \sigma(\phi_i^{Aj0} + W_{ji}^A) - \sigma(\phi_i^{Aj0} W_{ji}^A + \phi_i^B) \quad (3.4)$$

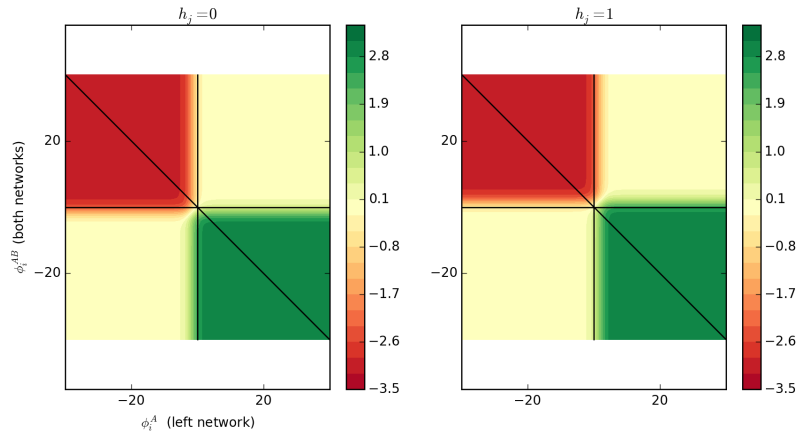


Figure 3.4: A diagram that shows the structure of the correction over the weighted sums into the hidden states of one of the RBMs versus both. Note the plateaus that are  $\pm \text{weight}$  in magnitude

### What happened to the biases?

The ORBM utilises the hidden biases present on the RBMs when calculating the hidden states  $h^A$  and  $h^B$ . However, the visible biases are not used in sampling from the visible. The reasoning behind this being that the RBMs visible bias acts like the ‘background rate’, i.e. what visible reconstruction would we see from an all zero hidden activation. As visible bias are not captured in the ORBM, it is important that RBMs plugged into it’s structure do not use a visible bias.

### Reconstructions and Dreams in the ORBM

Reconstructions in the ORBM are a natural extension of the inference algorithm.

- First hidden representations  $h^A$  and  $h^B$  are generated given an input  $v$ .
- The RBMs (RBM A and B) uses their respective hidden representations to generate visible patterns independently. That is, we can use the same way of performing Gibbs sampling we saw in equation 2.6.

This means that for a visible pattern there are potentially two reconstructions, one from each model.

## Chapter 4

# Design and Implementation

A significant hurdle for the project was gaining enough understanding of the existing work on RBMs to be able to implement the ORBMs algorithm and architecture. This was crucial as an incorrect implementation invalidates contributions 2 and 3 of this project.

### 4.1 Implementation Design

- Ordering of evaluation tasks made unit testing, with hand made test cases possible. Also less risk, remove the uncertainty around the RBM.
- testing approach

#### 4.1.1 Language Choice

*TODO WORDING* The implementation of the ORBM and inference algorithm is in *Python*, with *Matlab* and *Java* being the other languages considered.

I have spent my University career working in Java, and nowadays it is efficient to perform machine learning tasks. Python's module and class system promotes composition, and multiple inheritance in particular allows for composition of different classes.

Matlab is a popular numerical computing environment *TODO CITE*: and has a lot of on-line resources as well as machine learning papers *TODO CITE*: that include snippets or full Matlab programs that were used in the paper. Also Matlab is built around strong, efficient support for matrix operations which are very prolific in the RBM and ORBM implementations and evaluations.

Python has a very succinct syntax and shallow learning curve *TODO CITE*: , as well as being the language of choice of my supervisor. *TODO WORDING* This is favourable as I can have support for translating the algorithm into python correctly. Through libraries that supply wrappers for C-bindings, efficient code can be written but overall being an interpreted language Python is slower than Matlab and Java *TODO CITE*: . Three main factors influenced the choice for python:

**Up front learning** Given the amount of up front learning of concepts required to implement the solution, Python was favoured over Java or Matlab because it has a very shallow learning curve. Despite having experience in Java as well as Python, I had never used machine learning or linear algebra libraries in either languages. Given the amount of up front learning required to understand the concepts in this project let alone implement it, I opted for the shallower learning curve of Python. Also my supervisor has experience using Python and the libraries involved with this project. A shallower

learning curve meant that more time could be allocated to the evaluation which is the foremost contribution of this project.

**Library Support** Matlab and Python were two contenders in this factor, as a lot of matlab machine learning code is available with supporting papers [TODO CITE:](#) . Python has libraries such as NumPy, SciPy and Matplotlib [TODO CITE:](#) which mirror Matlabs functionality. However, NumPy and SciPy are all open source, while there is argument for treating an API as a black box — i.e. not writing code that is dependant on the underlying implementation, having the option to view source helped me better grasp the concepts. In particular being able to compare my implementation of the RBM to Sklearn's [TODO CITE:](#) allowed for some performance improvements.

**Ease of Evaluation** Python provides strong plotting library that is inspired by Matlab and R — Matplotlib [TODO CITE:](#) . Matplotlib is interoperable with the NumPy library, meaning that turning results into plots was really easy.

Also the evaluation requires repeatedly running a test to gain more confidence in the stochastic result. This is made possible by the ECS-Grid [TODO CITE:](#) . Python is supported with very minimal extra work required. A simple script that manages input and output is required. However the Java support on the ECS grid requires significantly more setup [TODO CITE:](#) . [TODO WORDING This seemed like an unnesccariy risk to introduce to the project at the later stage in the project where evaluation is being carried out.](#)

#### 4.1.2 Program Architecture

The implementation of the RBM, ORBM and algorithm is implemented with unit testing and composability in mind. It is important that the design supports comparing the Full and Approximated Correction [TODO CITE: Equation ...](#) By using Python, multiple inheritance could be leveraged to achieve this composability. For instance adding continuous pixel value support to the Full Correction Sampler, one simply needed to extend Continuous Approximate Correction Sampler and the Full Correction Sampler, with no code actually in the new class. The architecture is pictured in the class diagram 4.1. There were three main roles these classes filled:

1. The Trainer was used to train the weights of a supplied RBM. It would do so using a supplied sampler, decoupling how samples were generated from the training process.
2. The RBM was the model of an RBM, storing the weight matrix, as well as parameter information. Also this supported conversion of the SciPy Sklearn libraries' RBM implementation into the implementation used in this project. Decoupling the concept of an RBM from the Sampler and the Trainer meant that RBMs could be 'plugged' into the ORBM architecture with ease.
3. The Sampler defined how to perform Gibbs sampling, the subclasses defining whether it is standard RBM sampling or ORBM sampling. This made it trivial to compose samplers, which was required for the ORBM samplers.

#### 4.1.3 Testing Approach

The inference algorithm is the most crucial part of the implementation to test. In larger dimensional tasks, unit testing to ensure the algorithm produces the correct values becomes

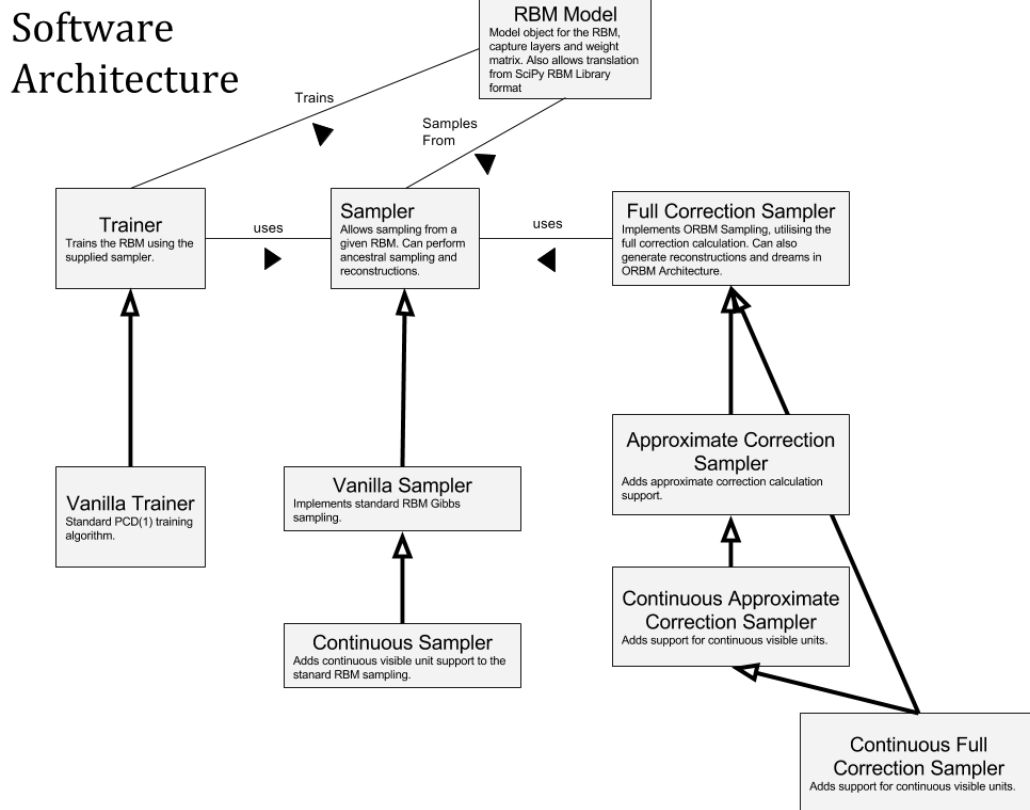


Figure 4.1: A figure showing the architecture for the implemented test suite in UML notation.

difficult. In smaller cases I was able to ensure the probabilities of  $P(h|v)$  and  $P(v|h)$  calculated by the implementation matches calculations I made by hand. Being an unsupervised black boxes, determining if an RBM (and by extension the ORBM) hidden representation is 'correct' for larger tasks such as the MNIST handwritten digit dataset is non-trivial. Concerned by this risk, I designed my evaluations to build confidence in the algorithm and the implementation.

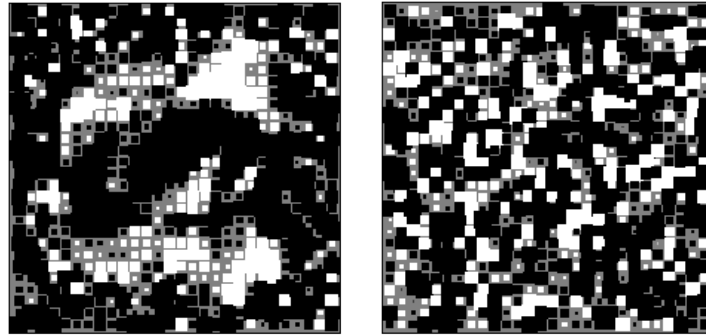
## 4.2 Evaluation Design: Evaluating RBMs and ORBMs

A challenge faced by this project and work with RBMs is that they are non-trivial to evaluate **TODO CITE:** . Being unsupervised black box, one cannot merely inspect the hidden units for an input and be sure that a good model has been learnt. As I plug RBMs into the ORBM architecture it is important for the overall results that the RBMs are well trained.

### 4.2.1 Hinton diagrams

We can examine the weights into a given hidden unit in the shape of the visible vector. For instance in the context of images, Hinton Diagrams allow visualisation of what a given hidden unit is 'doing' by visualising the matrix. This was first used by Hinton in the context of Boltzmann Machines in [7]. They also give insight into hidden unit utilisation. Weights are

often initialised to small random values resulting in a Hinton diagram with little structure to it. This is illustrated in figures 4.2a and 4.2b. The former showing a hidden units weights where some structure has been learnt, and the latter showing the opposite.



(a) Utilised hidden unit Hinton Diagram (b) Unutilised hidden unit Hinton Diagram

Figure 4.2: Hinton Diagrams illustrating a trained hidden unit, versus that of an untrained/unutilised hidden unit. This is with no measures to enforce sparsity.

#### 4.2.2 Reconstructions As a measure of Performance

Reconstructions, as described in Section 2.4.5, are a good measure of performance. **TODO CITE: Hinton showed this in papers, also cite more ppapers showing reconstruction use. starting from early RBM training papers by Hinton, up to more recent in deeper networks - the goal being to show the reader that reconstructions are used well in practice.** Given the precedent for using reconstructions as a performance measure, they will be the main way I evaluate the RBM in comparison to the ORBM.

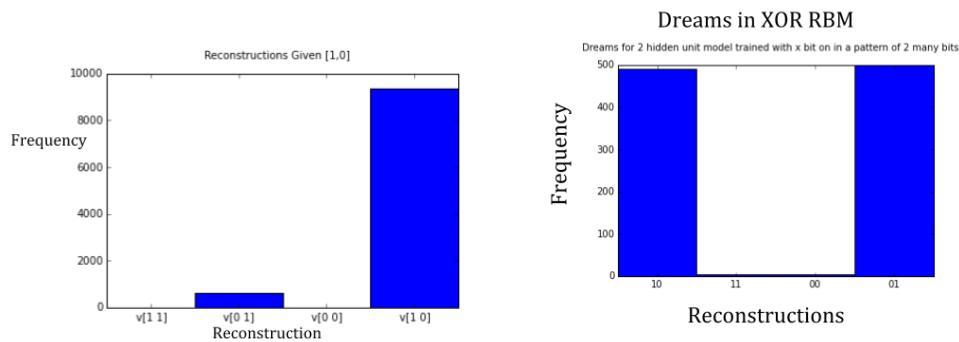
#### 4.2.3 Evaluating RBMs: Problem dependent

Evaluating RBMs is problem dependant, we can examine different the different approaches available by splitting problems into two cases:

**Problems with small dimentionality** When the dimentionality of the input is very small ( $< 10$ ) and all possible inputs are known we can perform analytical evaluations of the RBM. By clamping the visible units of the RBM to each input in the training set, reconstructions can be created. This process can be repeated for each input, recording the frequency that each reconstruction occurs on a bar graph. We can then ensure that the RBM is reconstructing the input perfectly. For instance, an RBM trained on two bit XOR and clamped to the input  $[1,0]$ , might have a bar graph of reconstructions as illustrated in figure 5.2.

In a similar way to the reconstructions, samples can be drawn from RBM in a ‘free phase’ without the input clamped to a given visible. The bar graph should exhibit dream visible patterns from the whole training set approximately an equal amount. Using the two bit XOR example once more, an example bar graph is shown in figure??.

**Problems with large dimentionalities** In non-trivial cases, with larger datasets, reconstructions can be inspected and compared to the training dataset. However, empirically detecting if a model is trained is difficult, especially given the unsupervised, black box nature of RBMs. Alternatively, a ‘score’ can be assigned to each item in the trainin



(a) Example reconstructions for the Handcrafted RBM, For 10000 independent reconstructions given the input  $[1, 0]$ . (b) Dreams in the XOR RBM, note how only the training data is present.

Figure 4.3: Bar graphs exemplifying the use of reconstructions and dreams for small numbers of RBMs.

set based on how well the RBM can reconstruct it. However in large cases your training set will not be complete — you will not have every possible valid image like you would in a case where your images are 2 pixels. Dreams can also be examined in larger cases, but again you cannot be as sure as in the smaller cases that you have a well trained RBM.

#### 4.2.4 Evaluation Methods

- Same models
- Growing dimensionality, bit strings to 2d to MNIST
- Allows comparison of Approx corrections in smaller scale - fail there don't continue using them...

TODO WORDING My TODO WORDING x experiments all followed the same high level process, working from trivial cases to more challenging tasks. The reasoning being that trivial cases make unit testing feasible, therefore ensuring conclusions can be drawn with regard to the algorithm and model, not an incorrect implementation. Also by incrementally increasing the difficulty of the task, it allows me to identify what qualities of the problem make the algorithm less or more effective.

#### Growing the complexity of evaluations

The evaluations in this project aimed to evaluate the ORBM and its inference algorithm by examining reconstructions given a multi-subject. Because the multi-cause inputs were images composed of known images, I could then compare the reconstructions to the ground truth.

An example of a multi-cause input with two quadrilaterals is shown in figure 4.4. The optimal reconstructions are equivalent to the two images that combined form the input.

In the smaller dimensional cases the reconstructions are inspected by hand, manually plotting the reconstructions and the frequency with which they occurred after a large amount of repetitions. In the larger dimensional tasks, two 'scores' were used to evaluate reconstructions against the training set.

To be able to use this reconstruction based evaluation, knowledge of the ground truth was required. This was so:

- RBMs could be trained and then plugged into the ORBM network.
- Reconstructions could be compared directly (by score) to the ground truth.

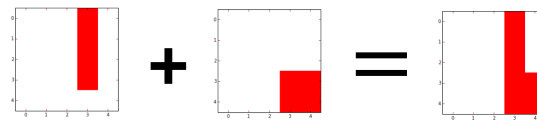


Figure 4.4: A figure illustrating two five by five pixel images combining to form a composite/multicause input. The images are binary.

#### 4.2.5 Choice of Evaluation Datasets

- 2 Bit XOR - It's the minimal case. Can examine reconstructions and dreams/fantasy empirically. Also can check that code performs as expected by manually calculating expected values for the algorithm.
- X Neighbouring Bits On in Y Bit Pattern - A natural next step from 2 bit XOR. Still trivial to train an RBM to represent, quick feedback to ensure the algorithm works. Allows comparing the different approximations tractable as number of hidden units is small enough.
- Square Patterns in a 5 by 5 Pixel Image - Another natural step from neighbouring bits, trivial to construct a dataset. Very easy to compose. Can use the same model for both models in the ORBM Architecture.
- Rectangles in a 5 by 5 Pixel Image - Next step, builds on the previous test but adds a different model for each source. Also different shapes of model can be used.
- Continuous Rectangles (Pixel values 0 to 1) in a 5 by 5 Image - Another variation working towards the MNIST dataset, same as the previous but has continuous visible pixels. Allows to different intensities, interesting cases where the images overlap and increase in intensity.
- MNIST Handwritten Digit Dataset - Pixel values from 0 to 1, 28 by 28 pixel image (784 pixel features.) Used extensively in previous studies. Gives me confidence that RBMs can learn these representations. Also allows metaparameters don't have to be tweaked as much as studies already have found reasonable values. Non-trivial to evaluate, but more of a real world case.

#### 4.2.6 Mixing Time Evaluation

- List the types Traceplot, Densityplots, Gelbin and Rubin multiple sequence diagnostics
- Examine hidden state, reconstructions as gibbs iterations occur.



## Chapter 5

# Evaluation

### 5.1 Two bit XOR: The minimal case

#### Description

The starting point for the evaluation is examining the ORBM reconstructions in a two bit pattern, where two of the same model were combining to form the data. This model made one bit on in a two bit pattern, i.e.  $[1, 0]$  or  $[0, 1]$ . The training set is the two bit XOR truth table and it provides the minimal case to compare the full correction calculation, versus that of the proposed approximation (see Equation 3.3 and 3.4 respectively).

#### Architecture and Parameters

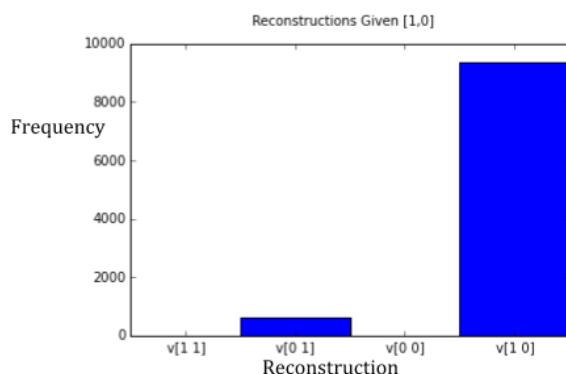


Figure 5.2: Example reconstructions for the Hand-crafted RBM, For 10000 independant reconstructions given the input  $[1, 0]$ .

shown in figure 5.2. The most common reconstruction is  $[1, 0]$ , which matches the input. We see that 500 reconstructions out of the 10,000 reconstructions are incorrect, corresponding to  $[0, 1]$ . This is due to the stochastic nature of the RBM, which is trained to increase the likelihood of training data, resulting in a small chance of producing reconstructions. This is

Being a trivial dimensionality, the RBMs weights were constructed by hand, meaning that only the ORBMs inference algorithm was being evaluated and not the training of the RBMs plugged into it. This network is picture in figure 5.1, [TODO WORDING with weights greater than 5](#) the networks stable state results in either  $[1, 0]$  or  $[0, 1]$ . The RBMs had 2 hidden units and 2 visible units.

#### Method

This RBM was checked to ensure that it behaved in practice by ensuring it's reconstructions matched the input for a large frequency of reconstructions. With the input  $[1, 0]$ , the results are

h

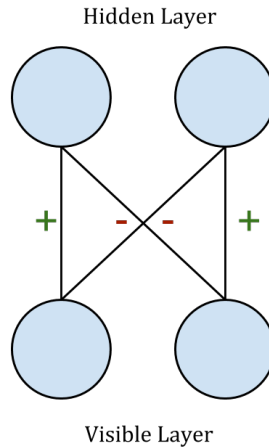


Figure 5.1: The two bit RBM for modelling a single bit on at a time in a two bit pattern. The diagonal weights are negative and the non-diagonal weights are positive.

Visible Input	Expected Reconstructions	
[1, 1]	[1, 0]	[0, 1]
[1, 0]	[1, 0]	[1, 0]
[0, 1]	[0, 1]	[0, 1]

Table 5.1: A Table showing the expected reconstructions from performing ORBM inference with various input patterns. The left and right hand column of the Expected Reconstructions column indicate the reconstructions from the left and right RBMs in the ORBM.

the why it is important to examine multiple reconstructions, especially in this small dimensionality where taking 10,000 samples is not time consuming (as it would be in tasks with larger dimensions).

In a similar way to the reconstructions, free-phase visible pattern samples can be taken from the model and evaluated. [TODO WORDING In larger dimensions Hinton has shown RBMs to be poor generative models without the extra layers above...](#) however in the small dimensions the dreams of the RBM should match the training set. A bar graph of frequencies of dreams is shown in figure 5.4. The RBM behaves as expected, generating dream patterns that match the training set in the correct proportion. With a valid model established, the XOR RBM was duplicated and plugged into the ORBM structure as illustrated in Figure 5.3.

The inference algorithm was run in the ORBM architecture for various visible inputs, giving two hidden vectors for the two representations  $h^A$  and  $h^B$ . For each pair of hidden vectors, a reconstruction was created, the process illustrated in figure 5.5. This process was repeated in a similar way to how the reconstructions were evaluated in the lone RBM, counting the frequency each reconstruction occurred over 1500 runs.

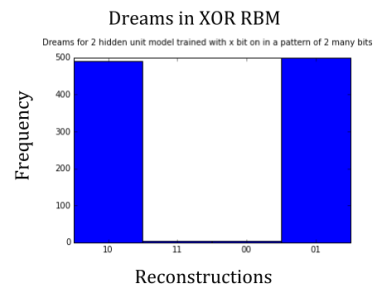


Figure 5.4: Dreams in the XOR RBM, note how only the training data is present.

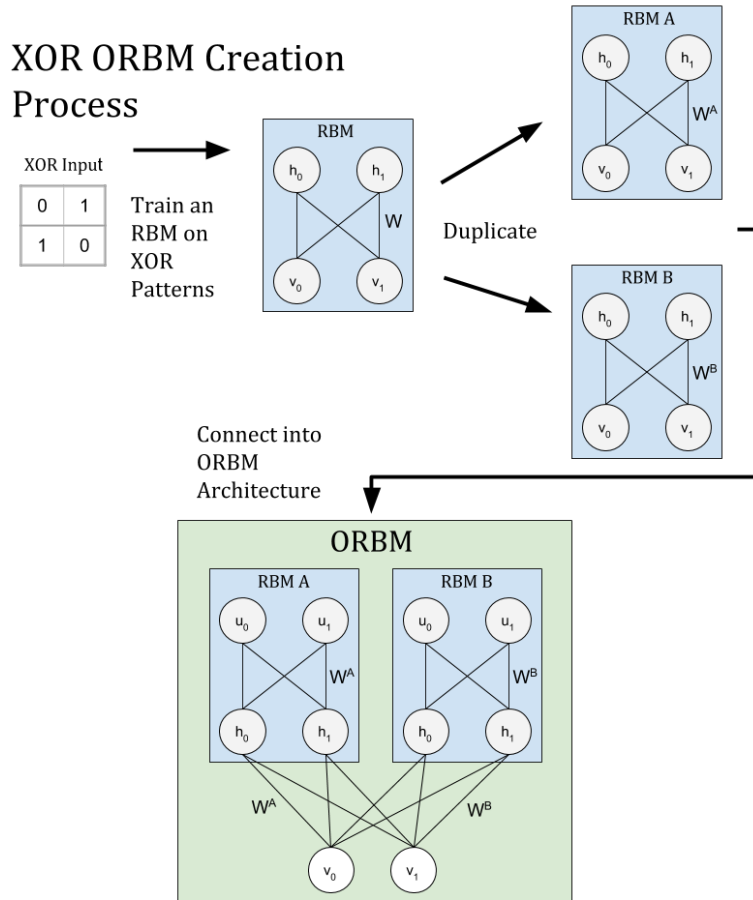


Figure 5.3: The process used to create the ORBM for evaluating composite XOR inputs.

### XOR ORBM Analysis

The results of this process are shown in figure ??.

Where the x-axis shows the reconstructions of the form A reconstruction, B reconstruction. The results show how applying the full correction compares to the approximated correction.

The ORBM is able to separate the causes with both types of correction, as the model is being duplicated, it produces  $[1, 0]$  and  $[0, 1]$  approximately half the time and symmetrically  $[0, 1]$   $[1, 0]$  the other half of the time. These reconstructions were compared to one of the RBMs trained to recognise a single pattern being on in two bits. As expected a machine that has been trained to recognise one bit, has no concept of two bits being on and hence the reconstructions show no mechanism for separating the sources. This is illustrated in figure 5.6.

The results of repeating this process with the input  $[1, 0]$  yielded successful results. We would hope that ORBM architecture could also handle inference with just a single subject. The results of this are shown in figure ??.

### Two bit XOR Conclusion

The ORBM was able to extract the target patterns  $[1, 0]$  and  $[0, 1]$  given the input  $[1, 1]$ . This was the case for both the Approximated and Full corrections, which gave confidence that the

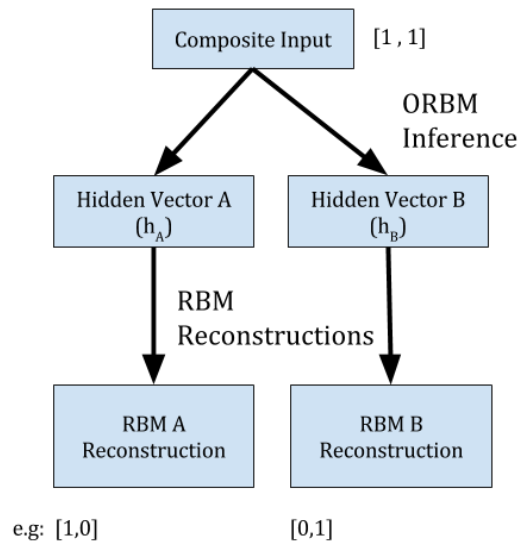


Figure 5.5: The process of generating reconstruction is shown in this diagram.

more computationally efficient Approximated correction could be relied on going forward — as for larger datasets it was a lot faster in practice. The generative model also copes with the subject overlapping, which in the two bit case arises when  $[1,0]$  is composed with  $[1,0]$ . In both the Approximated and Full corrections the highest occurring reconstruction is the target  $[1,0]$ , however there appears to be a lot less confidence.

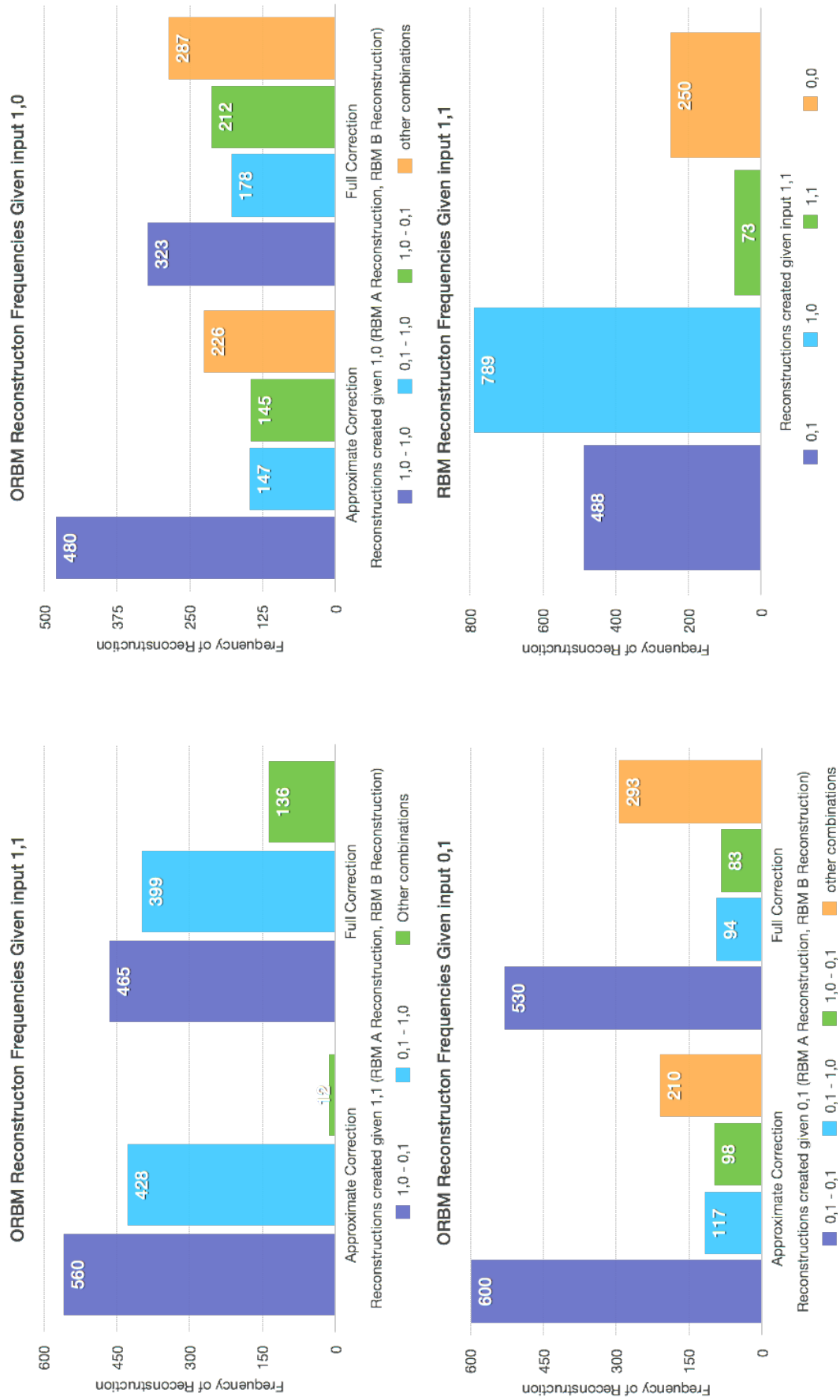


Figure 5.6: A figure showing the result of generating 1000 reconstructions with an RBM. It is clear the RBM has no mechanism to separate the sources. Hence showing it [1,1] when it has only been trained on XOR results in no separation, i.e. reconstructions including [1,1].

## 5.2 Y bit pattern, X neighbouring bits on

### Description

A natural next step from a single bit on in a 2 bit pattern, is moving up to  $X$  bits side by side on in a  $Y$  bit pattern is a next step. In affect this is modelling a  $X$  bit subject, in a  $Y$  bit pattern. For example if  $Y = 4$  and  $X = 2$  then a valid inputs are the rows of the following table:

$$dataset = \begin{bmatrix} 1 & 1 & 0 & 0 \\ 0 & 1 & 1 & 0 \\ 0 & 0 & 1 & 1 \end{bmatrix} \quad (5.1)$$

This allows for some interesting cases, for instance using the same example as above of  $Y = 4$  and  $X = 2$ , we can see how the ORBM is able to separate interesting patterns, for instance when the ‘subjects’ partially overlap such as  $[1, 1, 1, 0]$ , which is a composition of  $[1, 1, 0, 0]$  and  $[0, 1, 1, 0]$ . This evaluation will explore these interesting cases over a subset of the possible combinations of  $Y$  and  $X$ , ensuring that the ORBM is able to reconstuct the combination of images correctly.

### Architecture and Parameters

- $|Y|$  Hidden units per RBM, any less and we were unable to train the RBM to make the target reconstructions or dreams.
- Random normally distributed, mean and standard deviation of one, starting weights. The RBM was trained with 1000 epochs and a learning rate of 0.002.
- A sample of 10,000 dreams were sampled from the RBMs, and then plotted on a histogram in a similar fashion to figure ???. The frequency of produced dreams was ensured to be approximately equal and that the dreams should directly match the training set. This is feasible as the ground truth patterns are known.

### Method

For a subset of values of  $y \in Y, x \in X | 2 < x < y < 10$  the following process was repeated:

1. A single RBM was trained on all possible permutations of  $X$  neighbouring bits being on in a  $Y$  bit string (as seen in the Matrix 5.1).
2. The trained RBM was duplicated an plugged into the ORBM architecture.
3. For a subset of possible compositions of two patterns from xy [TODO WORDING list all combinations for a given xy to show infeasibility of doing them all](#) generate reconstructions using the ORBM. Where the cases examined are interesting cases such as partial and [TODO WORDING completely overallping and no overlapping](#)
4. Plot reconstructions on bar graphs ensuring they match the expected results.

### Results

A subset of the larger (but still small) dimension task results are shown in Figure 5.7. These illustrate the more interesting cases and the ORBM correctly separates the sources in all of them. The top left graph in Figure 5.7 extends the work in section 5.1 by recognising a single bit in a 5 bit pattern and the ORBM is sucessful. The top right graph illustrates the case of a

1 bit overlap of data made up of 2 neighbouring bits. The bottom left graph also exemplifies a 1 bit overlap but this time with a 'wider' pattern of 3 bits. The bottom right graph shows the case where the two 'subjects' are side by side, not overlapping. This is a disparity here that would likely be solved creating more reconstructions.

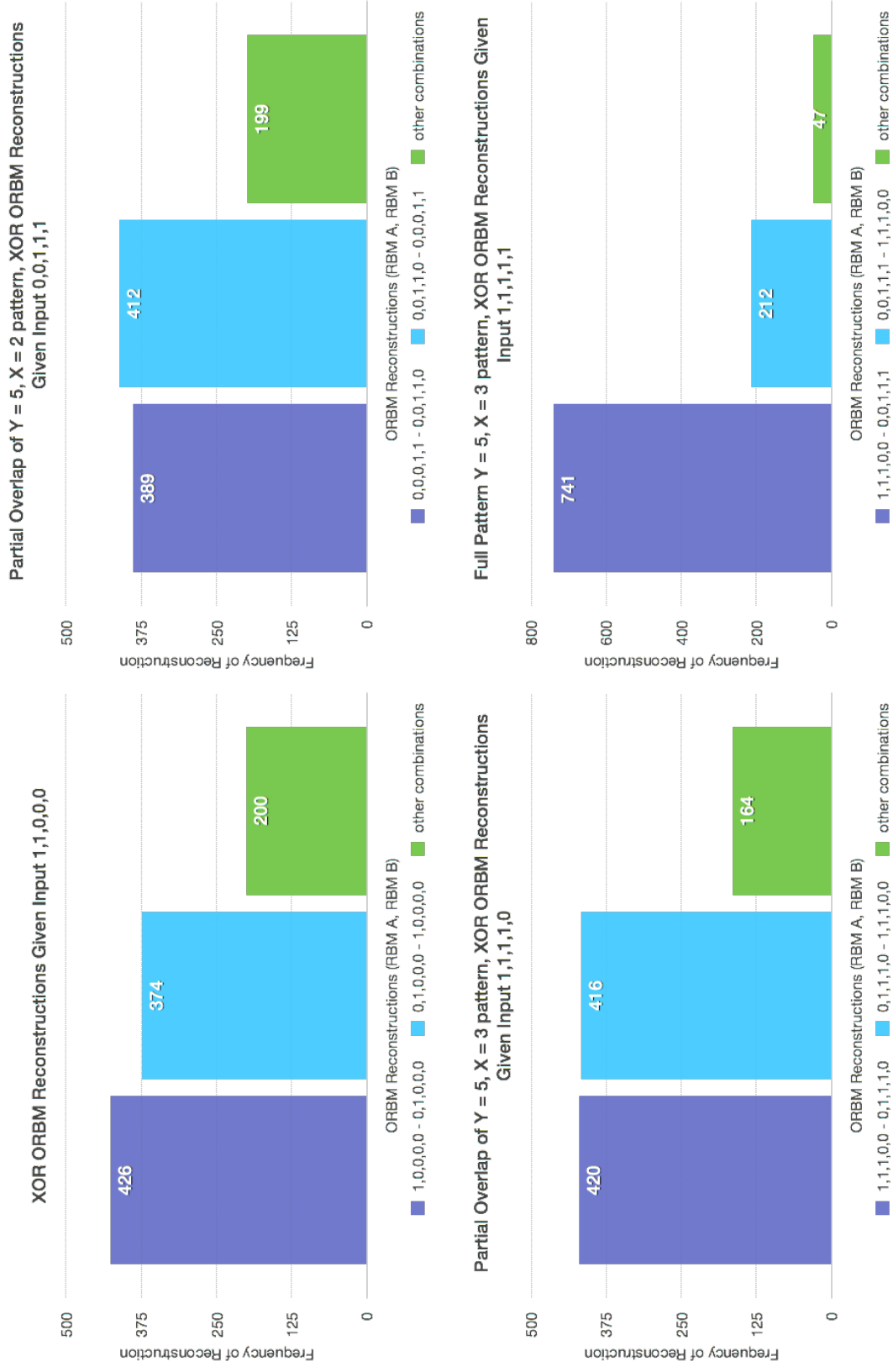


Figure 5.7: A figure showing interesting cases of ORBM reconstructions in Y bit pattern, X neighbouring bits on.



## 5.3 2D Patterns in a small dimensional space

### Description

For this task I am still working with a single RBM being duplicated, but now the dimensionality has increased to 25 in the form of a 5 by 5 pixel image.

### Architecture and Parameters

- Uses a 25 hidden unit RBM trained on a dataset of every permutation of a 2 by 2 square in a 5 by 5 pixel image. This is illustrated in Figure 5.8.
- The trained RBMs reconstructions and dreams were visually inspected, as well as Hinton diagrams to ensure an effective model.

### Method

The method followed a similar process as previous evaluations. Generate the training data, training and verifying the RBM to make sure it performed well. Next the whole dataset was composited with every other digit in that dataset, and ORBM reconstructions were then generated, as were RBM reconstructions. A subset of compelling results from this process are shown in Figure 5.9.

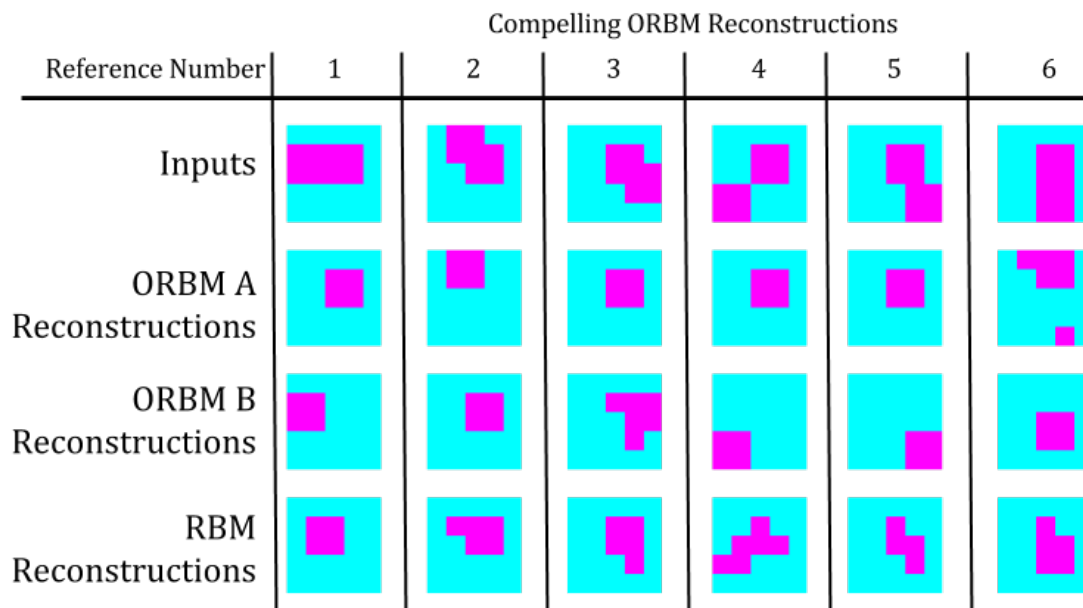


Figure 5.9: Figure illustrating a subset of the the results from ORBM inference on 2 By 2 square images.

- Dataset:
  - 2x2 square in a 5x5 image. Dataset of every possible configuration of said square.
- Method:

- train a single RBM to represent 2x2 squares in 5x5 space. Nice and small, can still inspect reconstructions, and dreams.
- Compose two square images with each other, can the ORBM architecture separate the images.

## 5.4 2D Pattern, Different Rectangle Separation

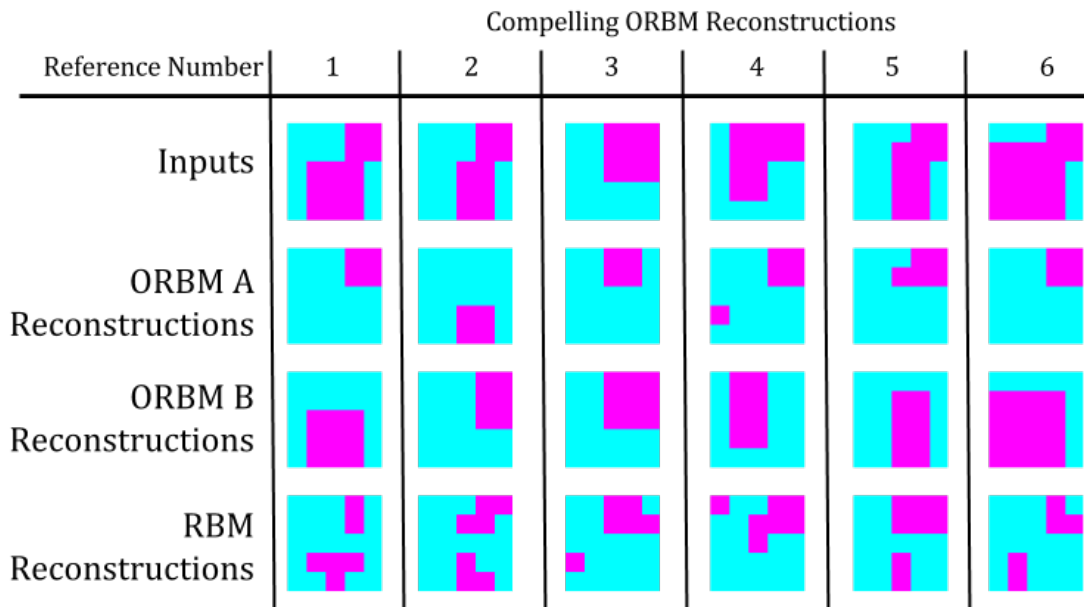
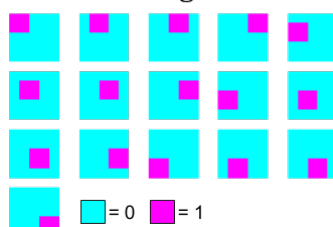


Figure 5.10: Figure illustrating a subset of the the results from ORBM inference on 2 by 2 squares combined with  $x$  by  $y$  pixel rectangles.

- Dataset
  - $n$  by  $m$  rectangles in 5x5 Images (TODO-IMAGE-IN-HERE) where  $n$  and  $m$  are not always equal.
- Method
  - Superimpose two images as the same way as before. How well can they separate.

## 5.5 MNIST Digits Mixing Time and Reconstructions

2 by 2 Squares in 5 by 5 Image



### Description

MNIST is a widely used dataset of handwritten digits (0 – 9). This task explored the non-trivial task of given two handwritten digits composited to form one image, how effectively can the ORBM separate the sources compared to the naive RBM? An example input is illustrated in figure [TODO CITE: ref.](#)

## Architecture and Parameters

### Architecture and Parameters

- MNIST Digit images are 28 by 28 pixel images, with pixel values between 0 – 1.
- 10, 100 Hidden unit RBMs trained on 500 examples of each digit respectively.
- Reconstructions and dreams of these RBMs were inspected by hand to ensure that they resembled the dataset.

### Method

For every digit dataset (of size 500), each digit in each dataset was composed with every other digit in every other dataset. Given this set of composite datasets, the corresponding RBMs were plugged in the ORBM architecture and used to create reconstructions. 100 Gibbs iterations were used when calculating the correction (generating the hidden states ( $h^A$  and  $h^B$ ) for a given input). These RBMs were also used to create standard RBM reconstructions. Given the ORBMs reconstructions (two per image) and the RBM reconstructions (also two per image) two scores were applied to compare these reconstructions to the ground truth:

**Cross Entropy** The cross entropy was calculated between the reconstruction and the ground truth.

**Cosine Angle** The angle between the flattened reconstruction vectors was computed, then negated to give a 'score'. The higher the score the smaller the angle between the reconstruction vector and the ground truth.

These scores can then be summed over each digit and over the entire dataset to find a single score for each digit composed with every other digit forming a 9 by 9 matrix. A cell of this matrix (say  $j, i$ ) corresponds to the difference between the ORBM score and RBM scores for digits  $j$  and  $i$  composited together. This entire process was repeated 10 times gain certainty in the results — given the stochasticity of the RBM and ORBM. This process is shown in Algorithm 2.

By finding the difference between the ORBMs reconstructions and the RBMs reconstruction we can create another matrix, in which a positive value represents a 'win' for the ORBMs reconstructions and a negative value represents a 'loss' (where the RBM outperformed the ORBM).

**Data:** MNIST Digit datasets, each with 500 examples, 10 RBMs trained on MNIST data 0–9 respectively

**Result:** Composite Datasets for every digit

**for** 10 repetitions to gain confidence in results **do**

**for** All MNIST digits datasets **do**

**for** Every digit example in the MNIST digit **do**

            composite the current digit dataset with every other dataset;

            Generate reconstructions on that dataset using the ORBM, RBM;

            Calculate the Cosine Angle score and Cross Entropy for both the RBM's and ORBM's reconstructions versus the ground truth;

**end**

        Sum the scores over every digit example;

**end**

    Tabulate the summed scores in a several matrices indexed by the digits being composited;

**end**

**Algorithm 2:** The algorithm explaining how the scores matrices were computed.

## Results

These score difference matrices are seen in for the Cross Entropy and Cosine Angle scores in 5.12a and 5.12b respectively, where the colour encodes the score. For the Cosine score, using the approximate correction, zero composed with every other digit yielded the best results for ORBM relative to the RBM, and nine the converse yielding particularly bad results (worse by a factor of 10 compared to zero). Given this, I plotted the RBMs Score versus the ORBM Score as a scatter plot, where each point corresponds to a score. This allows us to examine if the ORBM is performing worse as a whole, or if in some cases it is performing better than the RBM. These plots for zero and nine are shown in 5.13.

### 5.5.1 MNIST Analysis

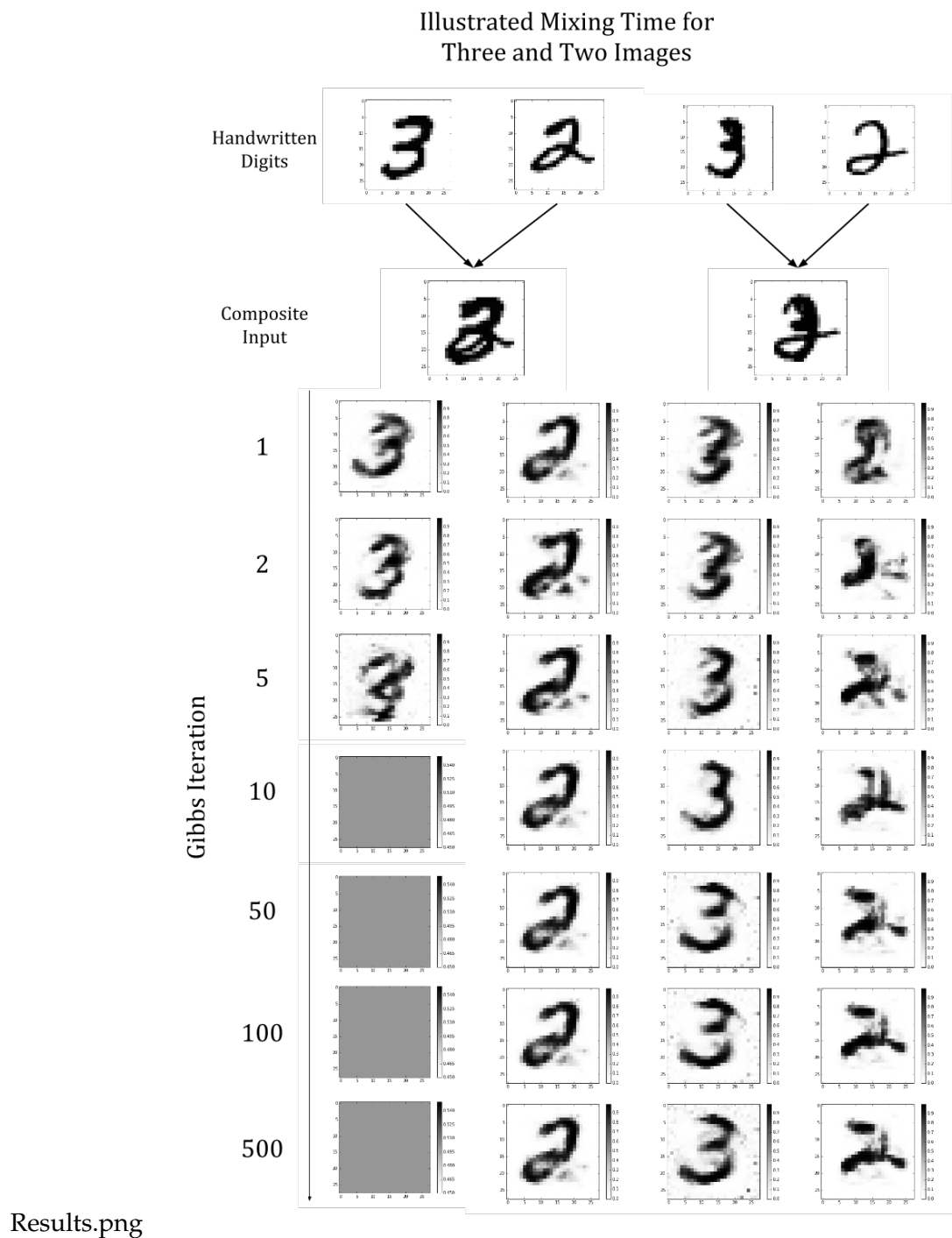
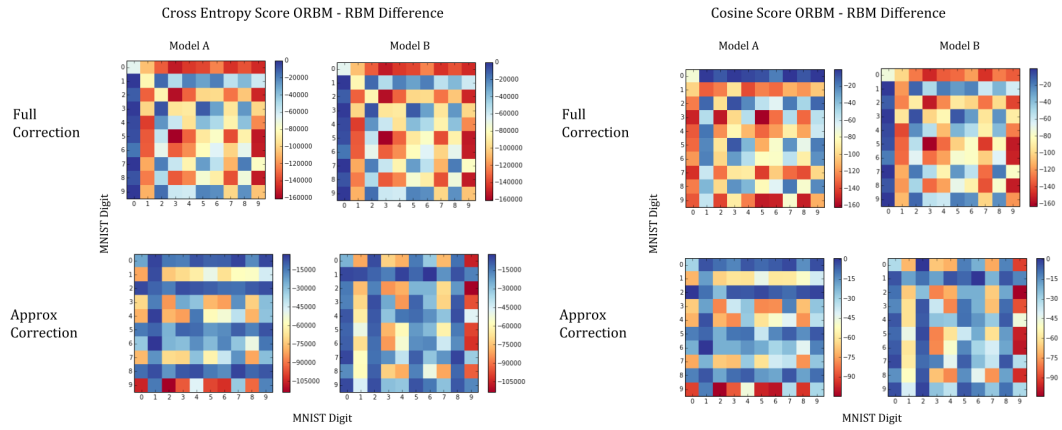


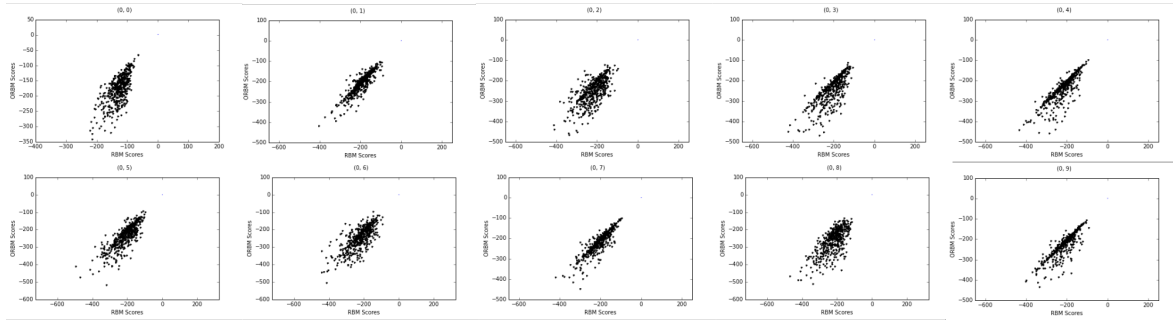
Figure 5.11: Mixing Time



(a) The cross entropy score summed over every item in the composite dataset. (b) The cosine score summed over every item in the composite dataset.

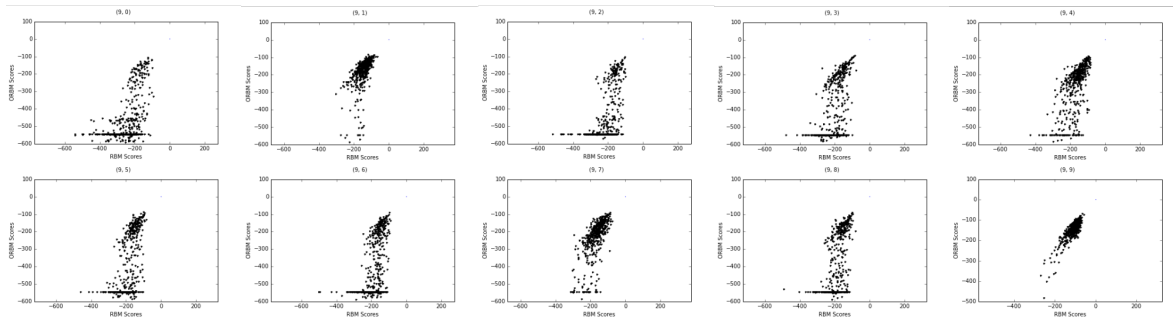
Figure 5.12: Dataset-wide MNIST Score Results

Reconstruction Scores for All Compositions of 0 and every other digit.



(a)  $(0, x)$

Reconstruction Scores for All Compositions of 9 and every other digit.



(b)  $(9, x)$

Figure 5.13: Cosine Score breakdown for the highest and lowest performing datasets, 0 and 9.

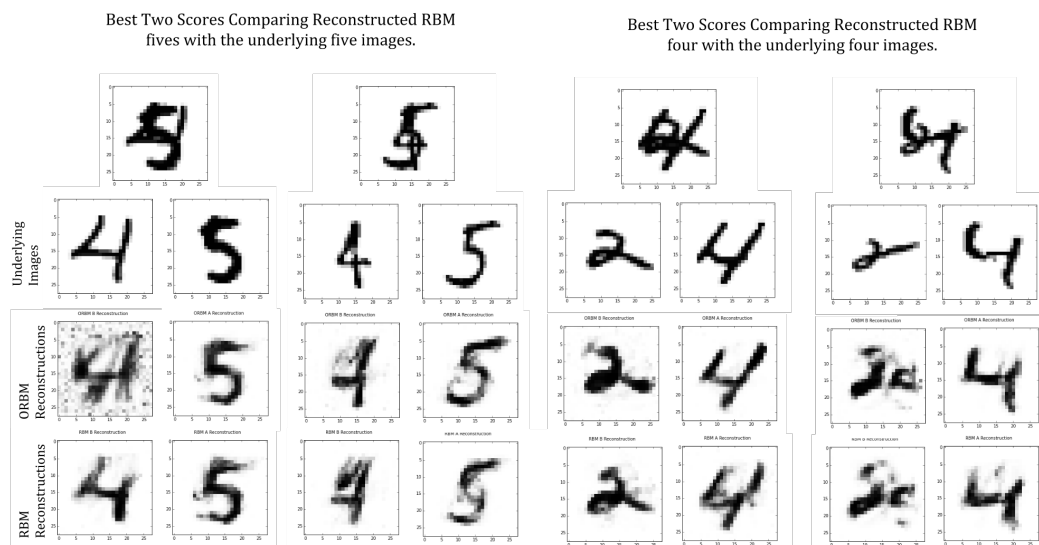


Figure 5.14: Best Scores

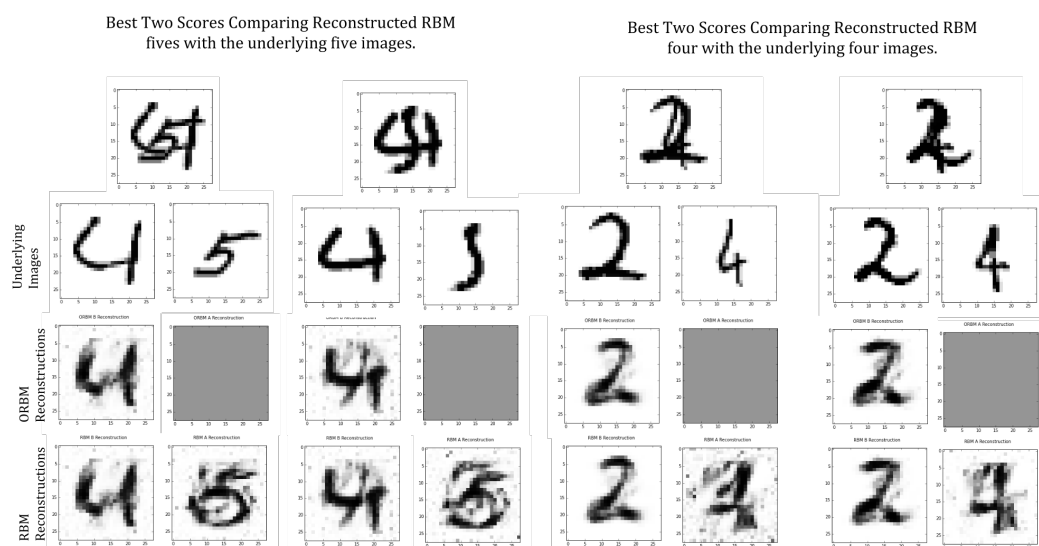


Figure 5.15: Worst Scores





## Chapter 6

# Conclusions and Future Work

- ORBM inference is working in smaller cases really well. Even better than the RBM!
- Training algorithm for this generative model has been proposed. Haven't been able to get it going but it could be really promising - Amounts to blind source separation.
- Disparity in weights between the models will have an effect. In trying to reaosn about why the activation would turn off it occurred to me that a disparity in weights between the models could allow one model overpower another! This could be overcome by moving back to a single model - and training MNIST 0-9 in one model and repeating the last experiment.
- No visible bias means that no activation in one model will make reconstructions incorrect for that model. But that is almost out of the scope for the ORBM.



# Bibliography

- [1] BARBER, D. *Bayesian Reasoning and Machine Learning*. Cambridge University Press, New York, NY, USA, 2012.
- [2] FISCHER, A., AND IGEL, C. Training restricted boltzmann machines: an introduction. *Pattern Recognition* 47, 1 (2014), 25–39.
- [3] HASTINGS, W. K. Monte carlo sampling methods using markov chains and their applications. *Biometrika* 57, 1 (1970), 97–109.
- [4] HINTON, G. E. To recognize shapes, first learn to generate images. *Progress in brain research* 165 (2007), 535–547.
- [5] HINTON, G. E., OSINDERO, S., AND TEH, Y.-W. A fast learning algorithm for deep belief nets. *Neural Comput.* 18, 7 (July 2006), 1527–1554.
- [6] HINTON, G. E., AND SEJNOWSKI, T. J. Analyzing cooperative computation. *Proceedings of the 5th Annual Congress of the Cognitive Science Society* (may 1983).
- [7] HINTON, G. E., AND SEJNOWSKI, T. J. Parallel distributed processing: Explorations in the microstructure of cognition, vol. 1. MIT Press, Cambridge, MA, USA, 1986, ch. Learning and Relearning in Boltzmann Machines, pp. 282–317.
- [8] HOPFIELD, J. J. Neural networks and physical systems with emergent collective computational abilities. *Proceedings of the National Academy of Sciences* 79, 8 (1982), 2554–2558.
- [9] JENSEN, C. S., AND KONG, A. Blocking gibbs sampling in very large probabilistic expert systems. *Internat. J. HumanComputer Studies* 42 (1995), 647–666.
- [10] NEAL, R. M. Connectionist learning of belief networks. *Artificial intelligence* 56, 1 (1992), 71–113.
- [11] PEARL, J. Reverend Bayes on inference engines: A distributed hierarchical approach. In *Proceedings of the American Association of Artificial Intelligence National Conference on AI* (Pittsburgh, PA, 1982), pp. 133–136.
- [12] PEARL, J. *Probabilistic Reasoning in Intelligent Systems: Networks of Plausible Inference*. Morgan Kaufmann Publishers Inc., San Francisco, CA, USA, 1988.
- [13] PEARL, J. *Probabilistic reasoning in intelligent systems: networks of plausible inference*. Morgan Kaufmann, 2014.
- [14] SMOLENSKY, P. *Foundations of harmony theory: Cognitive dynamical systems and the sub-symbolic theory of information processing*. Parallel distributed processing: Explorations in the ..., 1986.